SYSTEM IDENTIFICATION AND CONTROL OF SMART STRUCTURES: PANFIS MODELING METHOD AND DISSIPATIVITY ANALYSIS OF LQR CONTROLLERS

by

Soroush Mohammadzadeh

A Thesis

Submitted to the Faculty

of the

WORCESTER POLYTECHNIC INSTITUTE

in partial fulfilment of the requirements for the

Degree of Master of Science

in

Civil Engineering

May 2013

APPROVED:

Dr. Yeesock Kim, Thesis Advisor

Dr. Tahar El-Korchi, Committee Member and Head of Department

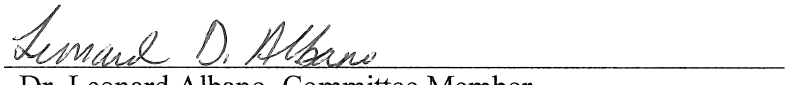

Dr. Leonard Albano, Committee Member

Abstract

Maintaining an efficient and reliable infrastructure requires continuous monitoring and control. In order to accomplish these tasks, algorithms are needed to process large sets of data and for modeling based on these processed data sets. For this reason, computationally efficient and accurate modeling algorithms along with data compression techniques and optimal yet practical control methods are in demand. These tools can help model structures and improve their performance. In this thesis, these two aspects are addressed separately. A principal component analysis based adaptive neuro-fuzzy inference system is proposed for fast and accurate modeling of time-dependent behavior of a structure integrated with a smart damper. Since a smart damper can only dissipate energy from structures, a challenge is to evaluate the dissipativity of optimal control methods for smart dampers to decide if the optimal controller can be realized using the smart damper. Therefore, a generalized deterministic definition for dissipativity is proposed and a commonly used controller, LQR is proved to be dissipative. Examples are provided to illustrate the effectiveness of the proposed modeling algorithm and evaluating the dissipativity of LQR control method. These examples illustrate the effectiveness of the proposed modeling algorithm and dissipativity of LQR controller.

Acknowledgements

I would like to thank Dr. Yeesock Kim, my thesis advisor for all his help, guidance and continuous support throughout my studies. Each of our weekly sessions was a learning opportunity for me, where Dr. Kim shared freely various concepts and techniques, for which to master, take a lot of time and effort. Dr. Kim also taught two courses that I enjoyed, challenging and hands-on: Structural Dynamics and Smart Structures. Dr. Kim also supported me in many situations, providing me with good advice and helpful information, being understanding, and letting me take a rewarding risk. I admire his management skills and appreciate his patience.

I would also like to thank Dr. Leonard Albano for his timely help on multiple occasions especially helping me achieve a great opportunity. I very much enjoyed our and gained insight into nature of Civil Engineering, teaching and being a student.

I would also like to thank Dr. Tahar El-Korchi for providing me with the opportunity to study at Worcester Polytechnic Institute.

I would also like to thank IAWPI for their help, support and great events.

Finally yet importantly, I would like to thank my parents, Majid and Robabeh, for their selfless devotion, help and support.

Table of Contents

List of Tables

List of Figures

1. Overview

Structural health monitoring and control is a branch of civil engineering science, which deals with identifying the status and properties of structures and controlling their behavior for a better performance under a variety of expected conditions. The purpose of structural health monitoring is to provide an understanding of the behavior of a structure or identify certain properties of a structure, which helps assess integrity, reliability and performance of the structure. In structural control, however, the focus is on improving the performance of a structure by modifying current structural elements or adding additional components if needed. The research outlined in the following thesis presents a new algorithm for structural health monitoring and a study on dissipativity of controllers used for control of civil structures.

Maintaining an efficient and reliable structure requires continuous monitoring and assessment of the state of its components. System identification can be used to model the behavior of a structure when it is equipped with a control device. An efficient non-parametric system identification method provides fast and accurate models of structures based on an input-output model framework, without the need for constructing detailed models as in finite element method. The challenge, however, is to create new algorithms for fast system identification. In this thesis, a new system identification method is proposed which is based on Principal Component Analysis (PCA). PCA is used to compress time-series input-output data of a structure, which reduces the computation time needed to create a model based on these data. This method can also be integrated in a structural control strategy.

As mentioned before, maintaining an efficient and reliable structure may demand improving its behavior under lateral loads using smart dampers. Smart dampers dissipate energy from a structure with real-time changeable damping properties. The challenge is to compute the optimal force, which is needed to be produced by the damper to decrease the vibration induced by lateral loads. LQR control method is commonly used to compute the optimal force. However, the optimal force needs to be dissipative; otherwise, the damper cannot produce the force.

This thesis encompasses the results of research conducted on two independent topics. A computationally efficient and accurate method of system identification is proposed and analyzed: PCA-based adaptive neuro-fuzzy inference system (PANFIS). Furthermore, a generalized definition of a dissipative force is proposed and the dissipativity of the LQR control method is proved, verified with simulation results and compared with PID method of control.

2. PCA-based neuro-fuzzy model for system identification of smart structures

2.1. Introduction

Smart control strategies constitute an important class of strategies used in the field of engineering (Housner *et al.* 1997, Spencer *et al.* 1997, Symans *et al.* 1999, Soong *et al.* 2002). The implementation of smart control devices such as magnetorheological (MR) dampers in structures has led to an increase in the buildings' ability to withstand destructive environmental forces such as strong winds or earthquake. However, it is generally known that even if the structure is assumed to behave linearly, there are nonlinearities introduced due to the implementation of various actuators and dampers (Kim *et al.*2009). Therefore, it is challenging to model the structure integrated with nonlinear actuators. Creating effective models for capturing nonlinear behavior of smart structures demands considerable amount of effort in terms of devising new models or using combinations of already available approaches as more efficient methods. With this in mind, this chapter proposes a method that efficiently identifies nonlinear behavior of seismically excited buildings equipped with smart dampers.

System identification (SI) is an essential part for synthesis of smart structures because it produces mathematical models for control system design using data measured from the structures. SI is used to reliably predict how a structure behaves using the inputs and outputs measured from the structure under a variety of dynamic loading scenarios such as far- and near-field earthquakes. SI can be separated into two categories: parametric and nonparametric approaches (Bani-hani *et al*. 1999). A parametric approach identifies the

properties of the structural system, including stiffness and damping elements that are intrinsically imbedded in the structure and its materials (Jalili-Kharaajoo 2004). The nonparametric SI method is used to train the input-output function of the structural system as a black box model (Filev 1991). It does not require accurate information about the structure. Thus, the nonparametric approach is easily applicable to nonlinear modeling of the structural system. This has successfully been performed with neural networks as well as fuzzy logic systems.

A fuzzy inference system, most commonly used as a nonparametric approach of modeling a system, uses fuzzy set theory to create a set of rules. It can be effective in dealing with nonlinearities and uncertainties of dynamic systems (Gu and Oyadiji 2008). Since the work of Zadeh (1965), fuzzy logic has been applied to many SI problems (Takagi and Sugeno 1985, Yan and Langari 1998, Kim *et al*. 2011). A number of studies on Takagi-Sugeno (TS) fuzzy models have been conducted in recent years, which deal with effective representations of nonlinear systems with the aid of fuzzy sets, fuzzy rules, and a set of local linear models (Filev 1991, Gopalakrishnan *et al*. 2010, Johansen and Babuska 2003). Fuzzy logic theory has been used mainly for nonlinear fuzzy control system design in the field of large-scale infrastructures (Guo *et al*. 2011, Kim et al. 2009, Mitchell *et al.* 2012). However, estimating the parameters of a fuzzy inference system requires many trials and errors. Hence, these fuzzy model parameters are determined using neural networks.

Development of artificial neural networks (ANN) was inspired by the cognitive mechanism of the human brain (Wang *et al.* 2009). The ANN consists of linked nodes. Each node computes an output from its input. The node output is then used as another input for other nodes, and a link is created between each node. ANNs improve the performance of each node by adjusting the parameters of the network, resulting in a more accurate model. Although ANN is effective in modeling nonlinear dynamic systems, it is challenging to design the ANN models in a transparent way because it is a black box modeling framework.

An integration of favorable features of both ANN and fuzzy logic models produces an effective nonlinear SI model, an adaptive neuro-fuzzy inference system (ANFIS). Its application for SI in civil engineering applications has been studied in many other researches; however, it still is a relatively new research topic (Gu and Oyadiji 2008, Gopalakrishnan 2010, Schurter *et al.* 2000, and Ozbulut *et al.* 2007). An advantage of this modeling technique is its ability to create effectively a nonlinear function using adjustable parameters, including types of the membership functions (MF), the number of MFs, step size of the learning process, and number of epochs. However, the ANFIS modeling technique can be computationally expensive or time-consuming (Wang *et al.* 2009). It would be disadvantageous when dealing with real-time situations and/or with large sets of data. To resolve these issues, principal component analysis (PCA) is incorporated in the ANFIS model to reduce the computation load.

PCA, first introduced in the context of data fitting by Pearson (1901), has been mainly used as a method for dimensional reduction of measurement data in diverse fields such as psychology, biology, chemistry, economics, genetics, and geology among other areas (Jollife 2002). Using this method, the contribution of each measurement to the variation of the whole data set can be determined. Such a process can be used to decrease the amount of data needed for further use by discarding redundant data or variables that are less important. There are some examples of implementation of PCA in the control and health monitoring field of civil engineering. Sharifi *et al*. (2010) applied PCA to sensor fault isolation and detection. Kuzniar and Waszczyszyn (2006) used PCA to identify natural periods from data measured from a building. Mujica *et al*. (2010) and Park *et al*. (2007) applied PCA to assess and detect damages in civil infrastructure.

The use of PCA as a means of data compression for an efficient training of an ANFIS model significantly reduces computation time. Warne *et al*. (2004) proposed a hybrid PCA-ANFIS measurement system for monitoring product quality in the coating industry by inferring the 'Anchorage' of polymer-coated substrates. Avci and Turkoglu (2009) proposed an intelligent diagnosis system based on PCA and ANFIS for the heart valve diseases. Polat and Gundes (2007) suggest using PCA and ANFIS together to diagnose lymph disease. These studies use PCA for dimensional reduction of large data sets, which are inherently different from time series of different types. In the previously proposed approaches, variables are combined together regardless of their type to find a combination with the maximum variance. However, input-output variables need to be separate when using ANFIS modeling technique, so that ANFIS can accurately capture the

effect of each input and output variable to produce a more accurate model. Therefore, the previously proposed approaches are not helpful for use in combination with ANFIS for modeling based on time series of various types. Compression of time series of various types using PCA for modeling with ANFIS, introduces a new challenge addressed in this chapter. In this work, PCA is implemented as a time series data compression method in which parts of the data are effectively removed during the compression process; however, the majority of the variation within the data is conserved for modeling purposes.

2.2. PCA-based adaptive neuro-fuzzy inference system (PANFIS)

PANFIS is an integrated model of PCA, ANN and fuzzy inference systems. It is a nonlinear learning model that uses a least-squares method as well as back-propagation methods to train the fuzzy inference system's MFs and its associated parameters using the PCA-based compressed input and output data sets.

2.2.1. Takagi-Sugeno fuzzy model

Takagi-Sugeno (TS) fuzzy model is the backbone for the proposed PANFIS control system. In 1985, Takagi and Sugeno proposed an effective way for modeling complex nonlinear dynamic systems by introducing linear equations in consequent parts of a fuzzy model, which is called a TS fuzzy model (Takagi and Sugeno 1985). It has led to the reduction of computational costs because it does not need any defuzzification procedures.

The fuzzy inference system used in the PANFIS model is of the TS fuzzy model form. It typically takes the following form

$$\begin{aligned} &R_j : IF\ u_{FZ}^1\ is\ P_{1,j}\ and\ u_{FZ}^2\ is\ P_{2,j} \ldots and\ u_{FZ}^i\ is\ P_{i,j} \\ &Then\ z_{FZ} = f_j\left(u_{FZ}^1,\ldots,u_{FZ}^i\right), j = 1,2,\ldots,N_r \end{aligned}, \tag{2-1}$$

where R_j is the j^{th} fuzzy rule, N_r is the number of fuzzy rules, $P_{i,j}$ are fuzzy sets centered at the operating j^{th} point, and u_{FZ}^i are premise variables that can be either input or output values. The equation of the consequent part $z_{FZ} = f_j(u_{FZ}^1,\ldots,u_{FZ}^i)$ can be any linear equation. Note that the equation (2-1) represents the j^{th} local linear subsystem of a nonlinear system, i.e. a linear system model that is operated in only a limited region. All of the local subsystems are integrated by blending operating regions of each local subsystem using the fuzzy interpolation method as a global nonlinear system

$$y_{FZ} = \frac{\sum_{j=1}^{N_r} W_j\left(u_{FZ}^i\right)\left[f_j\left(u_{FZ}^1,\ldots,u_{FZ}^i\right)\right]}{\sum_{j=1}^{N_r} W_j\left(u_{FZ}^i\right)}, \tag{2-2}$$

where $W_j\left(u_{FZ}^i\right) = \prod_{i=1}^{n} \mu_{P_{i,j}}\left(u_{FZ}^i\right)$ and $\mu_{P_{i,j}}\left(u_{FZ}^i\right)$ is the grade of membership of u_{FZ}^i in $P_{i,j}$. These parameters are optimized by the back propagation neural network. A typical architecture of fuzzy rules for a model with *n* membership functions for each input and n^2 rules is shown in Figure 2-1.

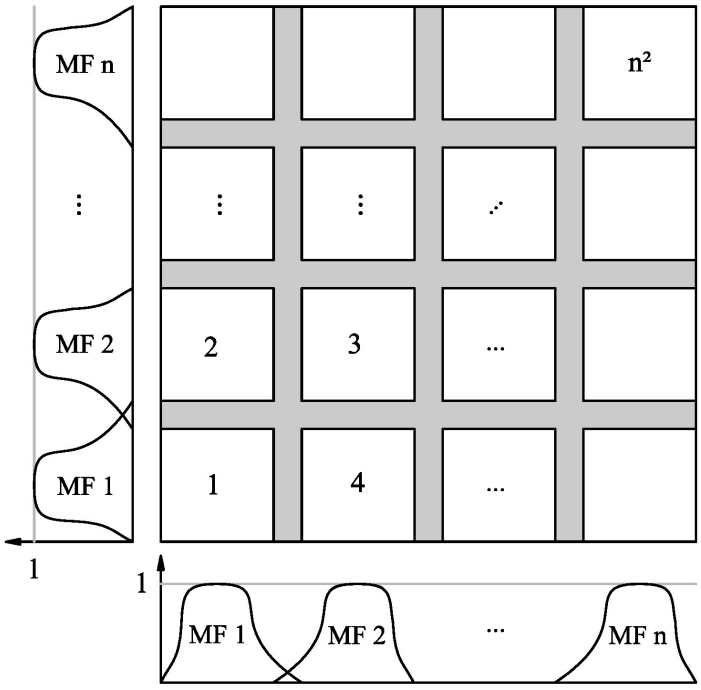

Figure 2-1. Typical fuzzy rules layout.

Optimization of the parameters of the model is the main challenge in the application of a fuzzy model. Therefore, incorporating neural networks to create an adaptive neuro-fuzzy inference system allows these parameters to be optimized during computation, which is explained below.

2.2.2. ANFIS ARCHITECTURE

The architecture of a typical ANFIS model is shown in Figure 2-2. This figure represents two inputs and one output architecture with *n* MFs for each input, which is only for illustrative purposes; the model used has two MFs for each input.

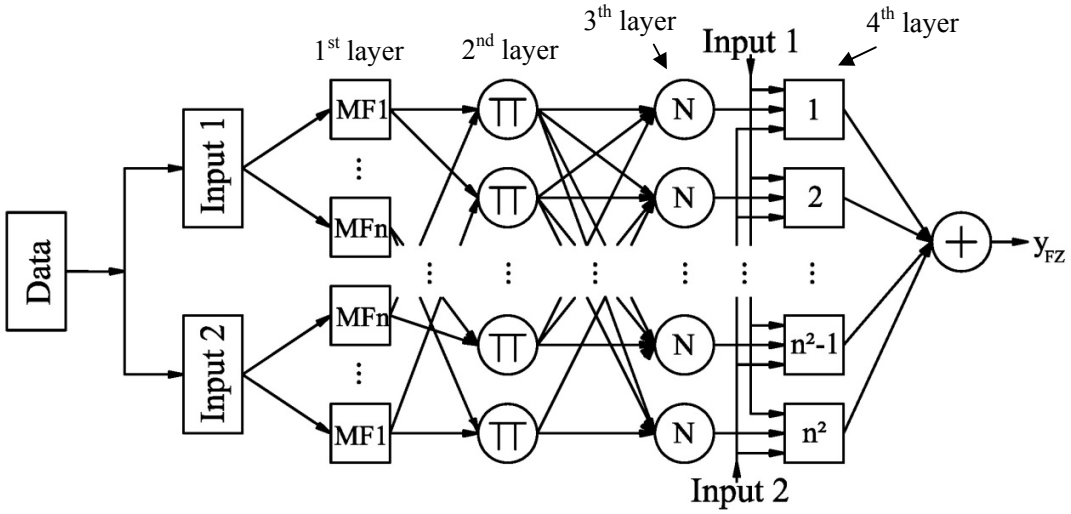

Figure 2-2. ANFIS architecture with *n* MFs for each of the two inputs.

Each layer has particular tasks to complete before the data moves to the next layer. In the first layer (layer 1), the function of the node is represented by

$$F_{FZ}^{1,j} = \mu_{P_{i,j}}\left(u_{FZ}^{i}\right), \tag{2-3}$$

The Gaussian MF used in the examples of this chapter has the following form

$$\mu_{P_{i,j}}\left(u_{FZ}^{i}\right) = \exp\left(-\left(u-a_1\right)^2 / 2a_2^2\right), \tag{2-4}$$

where a_1 and a_2 are adjustable parameters of the Gaussian function. This MF is applied to each input in layer 1. The second layer (layer 2) then outputs the product of all inputs of layer 2, known as the firing strengths

$$F_{FZ}^{2,j} = \mu_{P_{i,j}}\left(u_{FZ}^{1}\right) \times \mu_{P_{i,j}}\left(u_{FZ}^{2}\right) \ldots \mu_{P_{i,j}}\left(u_{FZ}^{i}\right), \tag{2-5}$$

The third layer (layer 3) takes a ratio of layer 2 firing strengths in order to normalize the layer 2 outputs $F_{FZ}^{2,j}$ as follows

$$F_{FZ}^{3,j} = F_{FZ}^{2,j} \Big/ \prod_{i=1}^{n} \mu_{P_{i,j}}\left(u_{FZ}^{i}\right). \tag{2-6}$$

The fourth layer (layer 4) then applies a node function to the normalized firing strengths

$$F_{FZ}^{4,j} = F_{FZ}^{3,j} \times f_j = F_{FZ}^{3,j}\left[f_j\left(u_{FZ}^{1},\ldots,u_{FZ}^{i}\right)\right], \tag{2-7}$$

where a_3, a_4 and a_5 are function parameters for the consequent. The last layer summates the layer inputs

$$F_{FZ}^{5} = \frac{\sum_j \prod_{i=1}^{n} \mu_{P_{i,j}}\left(u_{FZ}^{i}\right)\left[f_j\left(u_{FZ}^{1},\ldots,u_{FZ}^{i}\right)\right]}{\sum_j \prod_{i=1}^{n} \mu_{P_{i,j}}\left(u_{FZ}^{i}\right)}. \tag{2-8}$$

The output of the system F_{FZ}^{5} is then used in a hybrid learning algorithm to create a linear combination of the consequent parameters a_3, a_4 and a_5. The key parameters for this simulation include the number of iterations or epochs, the number of MFs and their type, as well as the step size of the function or algorithm. Types of MFs can vary from a generalized bell function, Gaussian functions, sigmoidal functions, trapezoidal function, as well as other forms. Each change of variables will yield different output results (Filev 1991 and Kim *et al*. 2011). The fuzzy inference system sets up rules based on the number of MFs used in simulation.

For a system with *n* MFs for each input, fuzzy rules are set up as shown in Figure 2-1, where y_{FZ} corresponds to F_{FZ}^{5}. Each number in layer 4 of Figure 2-2 represents one of the n^2 fuzzy regions that are created with *n* MFs in the ANFIS model. The fuzzy region is defined by the premise, and the output is generated through the consequent.

Although ANFIS is very effective in modeling complex nonlinear systems, it requires much computational effort. Such a problem can be addressed through the integration of principal component analysis.

2.2.3. *Principal component analysis (PCA)*

PCA was introduced by Pearson (1901) in the context of data fitting and was developed independently by Hotelling (Jollife 2002). Hotteling's method of derivation of principal components using Lagrange multipliers and eigenvalue/eigenvector analysis is explained in this section.

Suppose $\mathbf{v}_{obs.}$ is a matrix representing N observations of p random variables, organized as p rows and N columns, where the mean of random variable *i* is subtracted from each element of row *i*. The covariance matrix for this matrix of measurement data $\mathbf{v}_{obs.}$ can be constructed as

$$\mathbf{C}_{\mathbf{v}_{obs.}} = \frac{1}{N}\mathbf{v}_{obs.}\mathbf{v}_{obs.}^{T}, \tag{2-9}$$

where each element $c_{i,j}, i, j = 1,\ldots, p$ of the covariance matrix $\mathbf{C}_{\mathbf{v}_{obs.}}$, is the covariance between i^{th} and j^{th} variables. Element $c_{i,j}, i = j$ of the covariance matrix is the covariance between i^{th} and i^{th} variable which is the same as the variance of the i^{th} variable. It is often desirable to find a linear transformation of observation matrix $\mathbf{v}_{obs.}$, with the following form

$$\mathbf{V}_{tran.} = \mathbf{Q}\mathbf{V}_{obs.}\,, \tag{2-10}$$

which results in the maximum variances between linear combinations of p random variables among all other permissible linear combinations of them. $\mathbf{Q}$ is a transformation matrix. It is desirable for the transformation matrix $\mathbf{Q}$ to be a unit norm matrix, that is $\mathbf{Q}^T\mathbf{Q} = \mathbf{I}$. In other words, the goal is to find $\mathbf{Q}$, with the constraint $\mathbf{Q}^T\mathbf{Q} = \mathbf{I}$, such that the covariance matrix $\mathbf{C}_{\mathbf{V}_{tran.}}$ of the transformed set of data $\mathbf{V}_{tran.}$ is maximized,

$$\underset{\mathbf{Q}}{Max}\left\{\mathbf{C}_{\mathbf{V}_{tran.}}\right\}. \tag{2-11}$$

The function to be maximized, $\mathbf{C}_{\mathbf{V}_{tran.}}$ can also be written as

$$\mathbf{C}_{\mathbf{V}_{tran.}} = \frac{1}{N}\mathbf{Q}\mathbf{C}_{\mathbf{V}_{obs.}}\mathbf{Q}^T. \tag{2-12}$$

By employing the constraint condition, the objective function is formulated as follows

$$\frac{1}{N}\mathbf{Q}\mathbf{C}_{\mathbf{V}_{obs.}}\mathbf{Q}^T - \lambda(\mathbf{Q}^T\mathbf{Q} - \mathbf{I}), \tag{2-13}$$

where λ is the Lagrange multiplier. Differentiating with respect to $\mathbf{Q}$ gives

$$\left(\frac{1}{N}\mathbf{C}_{\mathbf{V}_{obs.}} - \lambda\mathbf{I}\right)\mathbf{Q} = \mathbf{0}, \tag{2-14}$$

where $\mathbf{I}$ is an $p \times p$ identity matrix, λ is an eigenvalue of the covariance matrix of the original data, and $\mathbf{Q}$ is found to be the corresponding matrix of eigenvectors of all the eigenvalues λ. Therefore, the eigenvectors of $\mathbf{C}_{\mathbf{v}_{obs.}}$ (i.e. $\mathbf{Q}$) transforms $\mathbf{C}_{\mathbf{v}_{obs.}}$ to a covariance matrix: the off-diagonal elements are zero and the diagonal elements have the maximum value. It is possible to examine each row as observations of random variables in

terms of their contribution (corresponding element in matrix of eigenvectors, $\mathbf{Q}$) to the covariance matrix. The variables with larger eigenvectors contribute more to the variation of the measurements. Therefore, it is possible to discard variables that contribute less than a threshold and decrease the dimensions of data needed for further analysis.

2.2.4. *PCA-based ANFIS system identification*

In the context of structural system identification, complex behavior of structures can be estimated using black box modeling framework with measured data. The measured data can include inputs and outputs to the structure. The input data may contain time series of earthquake signals and forces of control devices such as smart dampers. The output data may contain structural responses such as accelerations and displacements. In practice, the amount of measurement data for long periods can be huge. Hence, sometimes it is difficult to apply signal processing techniques (e.g. vibration analysis, system identification, structural health monitoring, control system designs, among others) to the lengthy data sets. Therefore, it is crucial to decrease the number of data points in these input-output time series. This can lead to a significant reduction in training time of ANFIS models or other machine learning techniques. The dimensional reduction approach mentioned in the previous section can be used to decrease the number of variables in input-output data sets (Warne *et al.* 2004, Avci *et al.* 2009, and Polat *et al.* 2007). In the context of structural system identification, the direct implementation of PCA to input-output data sets results in a linear combination of variables with different units (e.g. acceleration, displacement, force, etc.). However, the input-output variables need to remain separate, not combined, so

that ANFIS can capture the effects of each of the input and output variables to produce a more accurate model. Another implementation of PCA is suggested which is reasonable for use in this context.

Ground acceleration constitutes an important part of the inputs to the structure. To improve the computational efficiency of modeling, it seems reasonable to find only a short duration of ground acceleration within which large variations occur. These large variations may result in a broad range of behavior of the structure, which then helps to perform a more accurate and efficient system identification.

To find a short duration of earthquake signal with maximum variations among other durations, it is proposed to divide earthquake acceleration $\ddot{\mathbf{x}}_g(t), t \in [0,T]$ to N_t number of time series $\mathbf{v}_i(t), t \in \left[\frac{(i-1)}{N_t}T, \frac{(i)}{N_t}T\right], i = 1,...,N_t$ with equal lengths called segments, where each segment is small enough for favourable training time and large enough for reasonably accurate training of the ANFIS model. Then, PCA can be applied to the following matrix of the time series segments

$$\mathbf{v} = \begin{bmatrix} \mathbf{v}_1(0, \frac{1}{N_t}T) \\ \mathbf{v}_2(\frac{1}{N_t}T, \frac{2}{N_t}T) \\ \vdots \\ \mathbf{v}_N(\frac{N_t-1}{N_t}T, T) \end{bmatrix}, \tag{2-15}$$

to find principal components of the time series with the length of T/N_t.

Figure 2-3 represents the application of PCA to a time series. A five seconds long signal is divided into n segments using the window functions (applied point by point) and then the PCA is performed. The PCA coefficients (α_p) in (c) show where the important signal component is located within the whole data sets: indices of 1, 4, and $n-3$.

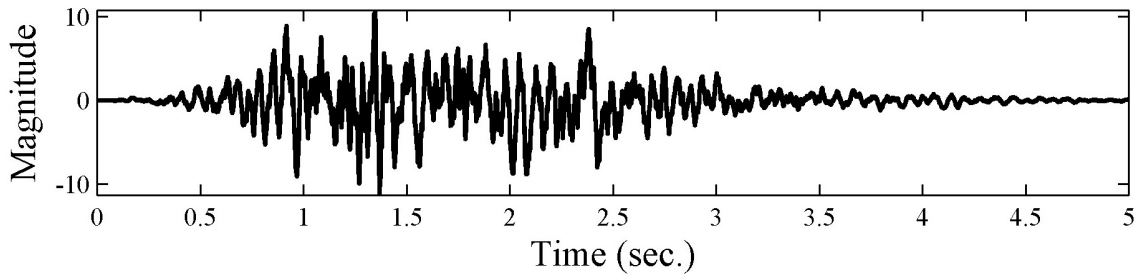

(a) An illustrative times series

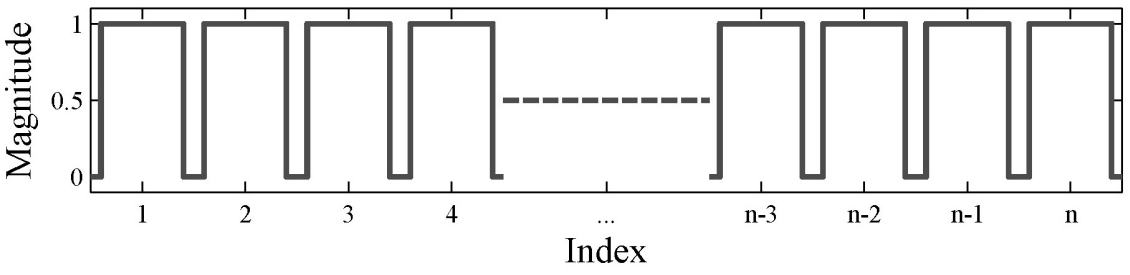

(b) Window functions

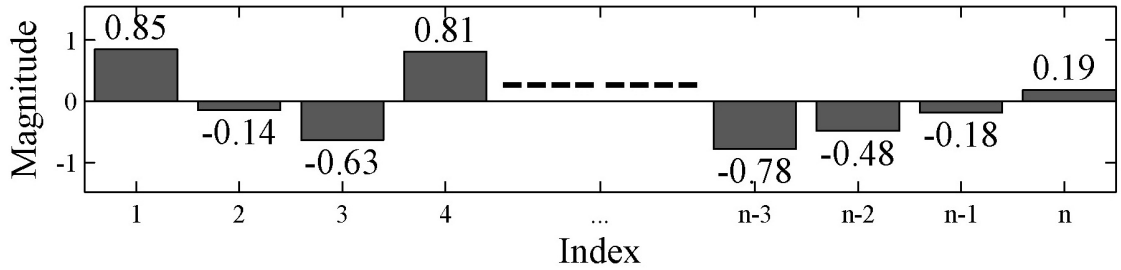

(c) PCA coefficient (α_p) for each segment

Figure 2-3. Application of PCA to times series

These results suggest that major contributions to the variation of the earthquake record is related to the data segments having an index of 1, 4 and $n-3$. Hence, instead of training the ANFIS model using the whole time series, the ANFIS model can be trained using segments added with the above PCA coefficients and the corresponding input-output segments. Therefore, the architecture of PANFIS can be as in Figure 2-4. It should be noticed that PCA is only applied to the earthquake time series to find the major contributing part, and the rest of the process of modeling is exactly the same as ANFIS, only the training data set is much smaller. In the following section, the effectiveness of the PANFIS modeling is demonstrated with examples.

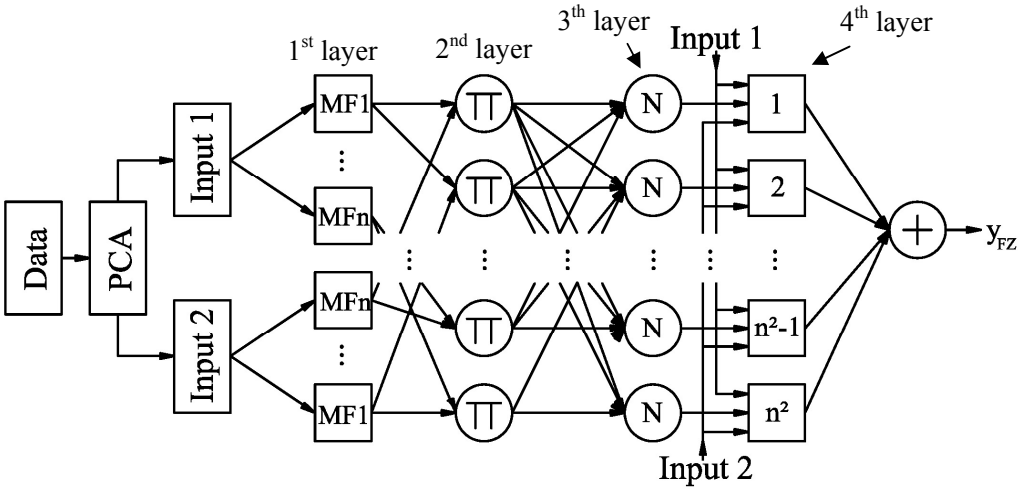

Figure 2-4. PANFIS architecture.

2.3. Example

To demonstrate the effectiveness of the PCA-based adaptive neuro-fuzzy inference system (PANFIS) approach, a three-story building structure equipped with a magnetorheological (MR) damper is investigated.

2.3.1. *Magnetorheological (MR) damper*

In recent years, smart structures have emerged from many engineering fields because the performance of structural systems can be improved without either significantly increasing the mass of the structure or requiring high cost of control power. They may be called intelligent structures, adaptive structures, active structures, and the related technologies adaptronics, structronics, etc. The reason to use these terminologies is that a smart structure is an integration of actuators, sensors, control units, and signal processing

units with a structural system. The materials that are commonly used to implement the smart structure: piezoelectrics, shape memory alloys, electrostrictive, magnetostrictive materials, polymer gels, magnetorheological fluid, etc. (Hurlebaus and Gaul 2006).

Semiactive control systems have been applied to large structures because the semiactive control strategies combine favorable features of both active and passive control systems. Semiactive control devices include variable-orifice dampers, variable-stiffness devices, variable-friction dampers, controllable-fluid dampers, shape memory alloy actuators, piezoelectrics, etc. (Hurlebaus and Gaul 2006). In particular, one of the controllable-fluid dampers, magnetorheological (MR) damper has attracted attention in recent years because it has many useful characteristics.

In general MR dampers consists of a hydraulic cylinder, magnetic coils, and MR fluids that typically contain micron-sized magnetically polarizable particles floating within oil-type fluids as shown in Figure 2-5. The MR damper can be operated as a passive damper; however, when a magnetic field is applied to the MR fluid, the fluid changes into a semi-solid state in a few milliseconds. This is one of the most unique aspects of the MR damper compared to active systems: malfunction of an active control system might occur if some control feedback components, e.g., wires and sensors, are broken for some reasons during severe earthquake event; while a semiactive system can still be operated as a passive damping system even when the control feedback components are not functioning properly. Its characteristics are summarized in (Kim *et al*. 2009).

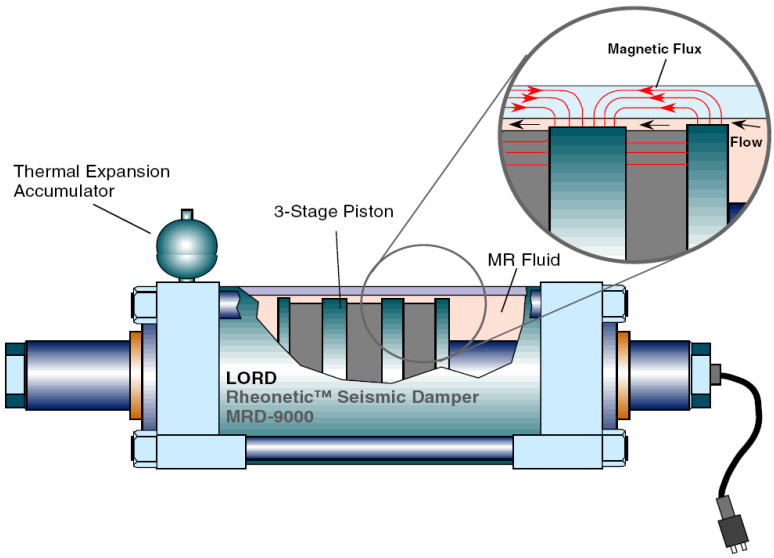

Figure 2-5. Schematic of the prototype 20-ton large-scale MR damper (Yang *et al.* 2002).

To fully exploit the behavior of MR dampers, a mathematical model is needed that portrays the nonlinear behavior of the MR damper. However, this is challenging because the MR damper is a highly nonlinear hysteretic device. As shown in Figure 2-6, the MR damper force $f_{MR}(t)$ predicted by the modified Bouc-Wen model is governed by the following differential equations. Spencer et al. (1997) provides more detailed discussion of this model.

$$f_{MR} = c_a \dot{u}_b + k_a (u_a - u_{a_0}), \tag{2-16}$$

$$\dot{z}_{BW} = -\gamma |\dot{u}_a - \dot{u}_b| z_{BW} |z_{BW}|^{n-1} - \beta (\dot{u}_a - \dot{u}_b) |z_{BW}|^n + A(\dot{u}_a - \dot{u}_b), \tag{2-17}$$

$$\dot{u}_b = \frac{1}{(c_a + c_b)} \{\alpha z_{BW} + c_b \dot{u}_a + k_b (u_a + u_b)\}, \tag{2-18}$$

$$\alpha = \alpha_a + \alpha_b u_{MR}, \tag{2-19}$$

$$c_a = c_{a_1} + c_{a_2} u_{MR}, \tag{2-20}$$

$$c_b = c_{b_1} + c_{b_2} u_{MR}, \tag{2-21}$$

$$\dot{u}_{MR} = -\eta(u_{MR} - v_{MR}). \tag{2-22}$$

where z_{BW} and α called evolutionary variables, describe the hysteretic behavior of the MR damper; c_b is the viscous damping parameter at high velocities; c_b is the viscous damping parameter for the force roll-off at low velocities; α_a, α_b, c_{b_1}, c_{b_2}, c_{a_1} and c_{a_2} are parameters that account for the dependence of the MR damper force on the voltage applied to the current driver; k_b controls the stiffness at large velocities; k_a represents the accumulator stiffness; u_{a_0} is the initial displacement of the spring stiffness k_a; γ, β and A are adjustable shape parameters of the hysteresis loops, i.e., the linearity in the unloading and the transition between pre-yielding and post-yielding regions; v_{MR} and u_{MR} are input and output voltages of a first-order filter, respectively and η is the time constant of the first-order filter.

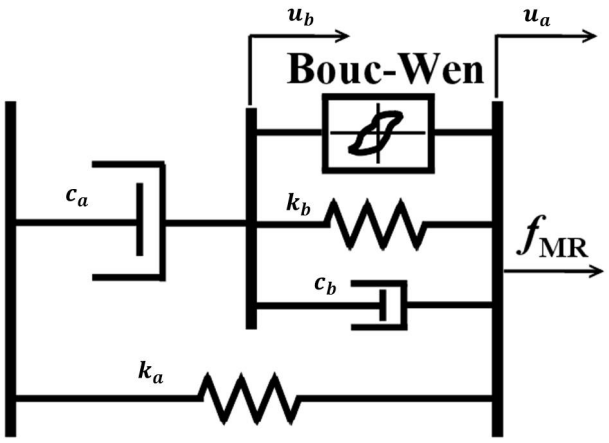

Figure 2-6. Modified Bouc-Wen model of the MR damper (Spencer *et al*. 1997).

The structure itself is assumed to behave linearly; however, the addition of the MR damper introduces nonlinearities, which necessitate developing a mathematical model to portray this behavior, which is usually the key part in the design of semiactive control systems.

2.3.2. *Integrated structure-MR damper system*

A typical example of a building structure employing an MR damper is depicted in Figure 2-7.

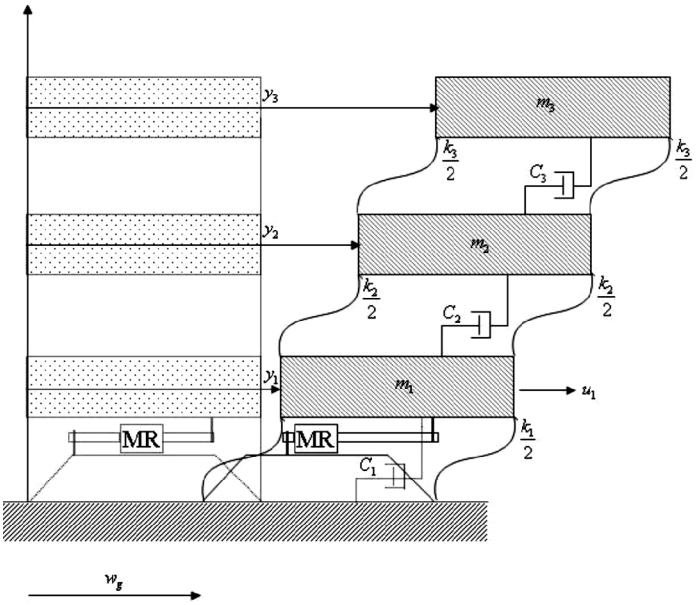

Figure 2-7. A three-story building employing an MR Damper (Kim *et al.* 2011).

The associated equation of motion is given by

$$\mathbf{M}\ddot{\mathbf{x}} + \mathbf{C}\dot{\mathbf{x}} + \mathbf{K}\mathbf{x} = \mathbf{\Gamma}\mathbf{f}_{MR}(t, \mathbf{x}_i, \dot{\mathbf{x}}_i, v_{MR_i}) - \mathbf{M}\mathbf{\Lambda}\ddot{x}_g , \tag{2-23}$$

where $\ddot{x}_g$ denotes the ground acceleration; $\mathbf{M}$ the mass matrix, $\mathbf{K}$ the stiffness matrix, $\mathbf{C}$ the damping matrix, and the vector $\mathbf{x}$ the displacement relative to the ground, $\dot{\mathbf{x}}$ the velocity, $\ddot{\mathbf{x}}$ the acceleration; $\mathbf{x}_i$ and $\dot{\mathbf{x}}_i$ are the displacement and the velocity at the i^{th} floor level relative to the ground, respectively; v_{MR_i} is the voltage level to be applied; also $\mathbf{\Gamma}$ and $\mathbf{\Lambda}$ are location vectors of control forces and disturbance signal, respectively. The second order differential equation can be converted into a state space model

$$\begin{aligned} \dot{\mathbf{z}} &= \mathbf{A}\mathbf{z} + \mathbf{B}\mathbf{f}_{MR}(t, \mathbf{x}_i, \dot{\mathbf{x}}_i, v_i) - \mathbf{E}\ddot{x}_g \\ \mathbf{y} &= \mathbf{C}\mathbf{z} + \mathbf{D}\mathbf{f}_{MR}(t, \mathbf{x}_i, \dot{\mathbf{x}}_i, v_i) + \mathbf{n} \end{aligned} , \tag{2-24}$$

in which the following parameters are used

$$\mathbf{A}=\begin{bmatrix}\mathbf{0} & \mathbf{I}\\ -\mathbf{M}^{-1}\mathbf{K} & -\mathbf{M}^{-1}\mathbf{C}\end{bmatrix}, \tag{2-25}$$

$$\mathbf{B}=\begin{bmatrix}\mathbf{0}\\ \mathbf{M}^{-1}\mathbf{F}\end{bmatrix}, \tag{2-26}$$

$$\mathbf{C}=\begin{bmatrix}\mathbf{I} & \mathbf{0}\\ \mathbf{0} & \mathbf{I}\\ -\mathbf{M}^{-1}\mathbf{K} & -\mathbf{M}^{-1}\mathbf{C}\end{bmatrix}, \tag{2-27}$$

$$\mathbf{D}=\begin{bmatrix}\mathbf{0}\\ \mathbf{0}\\ \mathbf{M}^{-1}\mathbf{F}\end{bmatrix}, \tag{2-28}$$

$$\mathbf{E}=\begin{bmatrix}\mathbf{0}\\ \mathbf{F}\end{bmatrix}, \tag{2-29}$$

where $\mathbf{F}$ is the location matrix of Chevron braces within the building structure, $\mathbf{n}$ is the noise vector, $\mathbf{x}_i$ and $\dot{\mathbf{x}}_i$ are the displacement and the velocity at the i^{th} floor level of the three-story building structure, respectively. Properties of the three-story building structure are adopted from Dyke *et al.* (1996).

2.3.3. *Simulation*

To demonstrate the effectiveness of the PANFIS model, a set of input-output data is generated from a building structure equipped with an MR damper, illustrated in Figure 2-8. The approach proposed in Section 2.2. is then applied, i.e. PCA is first used to compress the five-seconds-long artificial earthquake signal to a one-second-long signal. The segments of the signal along with the corresponding PCA coefficients (α) are illustrated in Figure 2-9. It should be noted that the sum of squares of the PCA coefficients is equal to one. In this example, the two components (b) and (c) of artificial earthquake shown in

Figure 2-9 are used with the corresponding MR damper forces and acceleration responses to train the ANFIS model, reducing the computation load significantly.

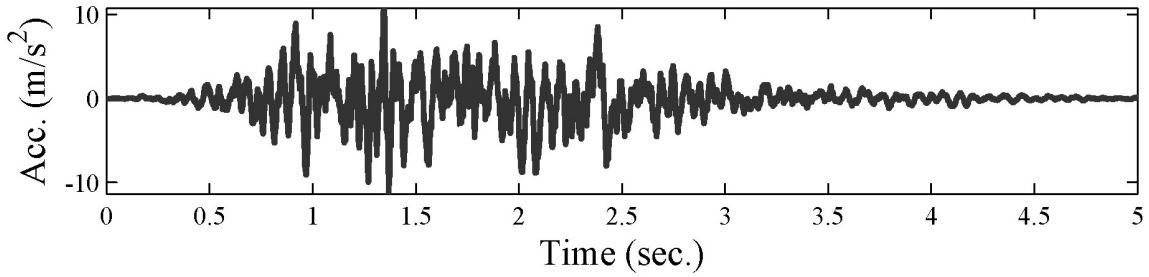

(a) Artificial earthquake

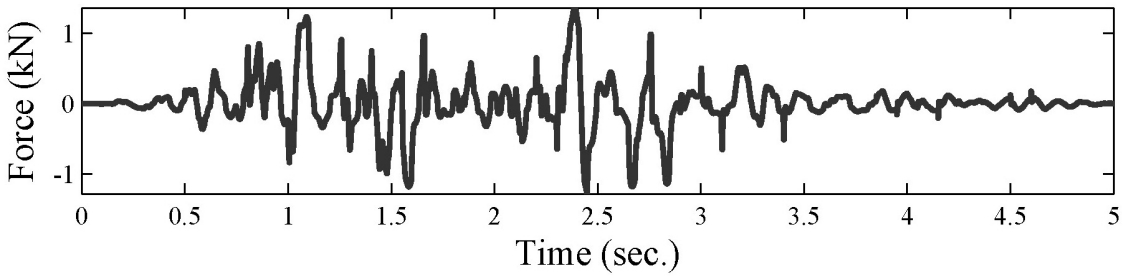

(b) MR damping forces

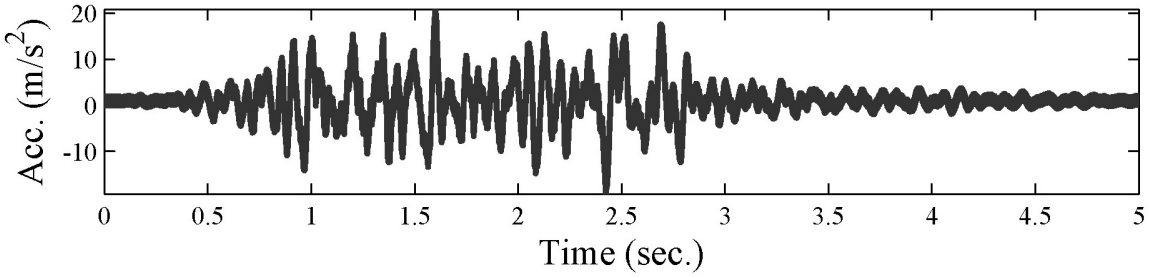

(c) Structural responses

Figure 2-8. A set of input and output for training the PANFIS model.

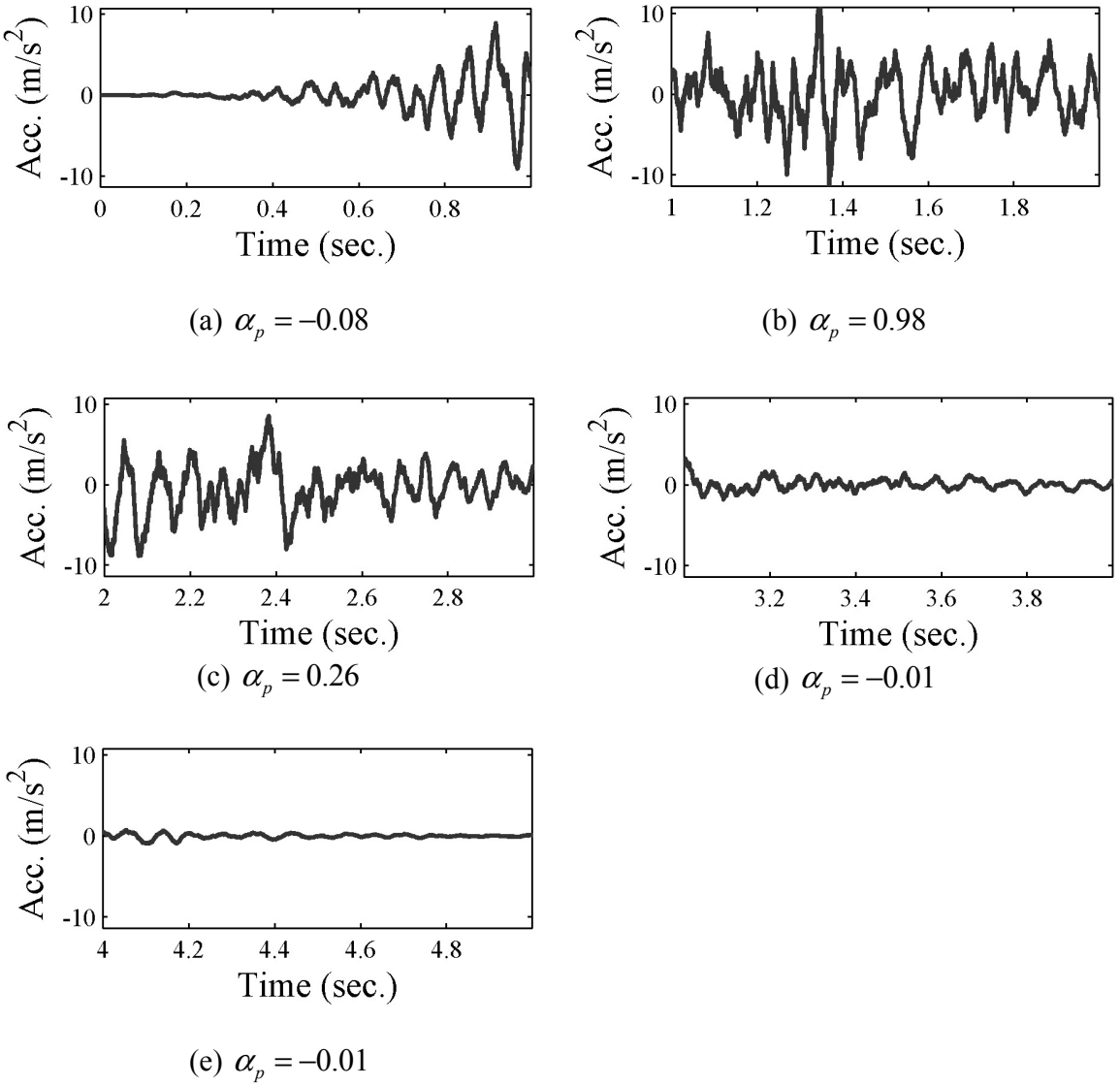

Figure 2-9. Five segments of the artificial earthquake with corresponding PCA coefficients.

The architecture of the PANFIS model is determined via trial-and-error. The number of MFs used in the model was increased from two to eight for both earthquake and

MR damper force and two MFs for each was found to be resulting in accurate and efficient model. Gaussian MFs are used as the design variables. Maximum number of epochs is 150 and the step size is chosen as 0.001. Although the architecture of the PANFIS model can be optimized through an optimization procedure, it is beyond the scope of the present chapter.

Figure 2-10 compares the dynamic response of the original simulation model with that of the trained PANFIS model. Note that the original simulation model is an analytical model of the building equipped with an MR damper subjected to the artificial earthquake signal. As seen, overall good agreements between the original data and the identified PANFIS model is found. The modeling errors are quantified using indices defined later. As previously discussed, the performance of the PANFIS model can be improved by increasing input parameters, which can also significantly increase computation time.

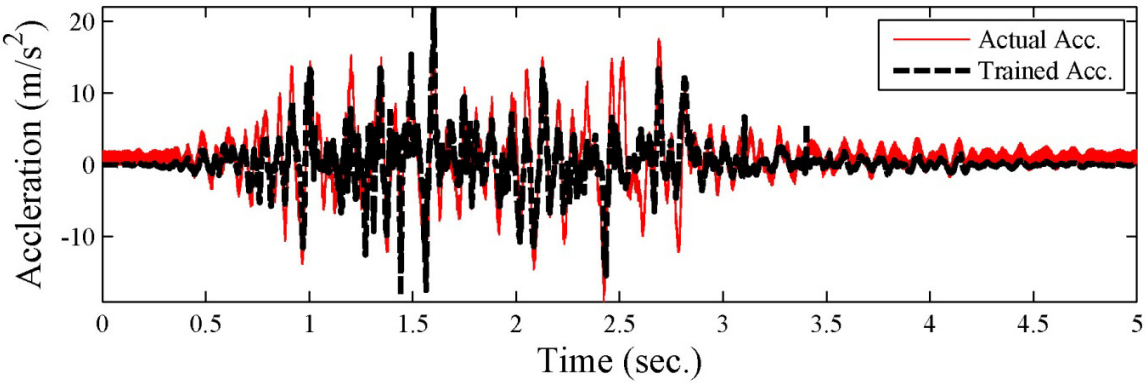

Figure 2-10. Training: Artificial earthquake.

It is necessary to validate the trained model using data that have not been used for training the model to assess whether the trained model can be used for a range of possible earthquakes. Figures 2-11 through 2-14 show the four earthquake signals for the validation: El Centro, Kobe, Hachinohe, and Northridge.

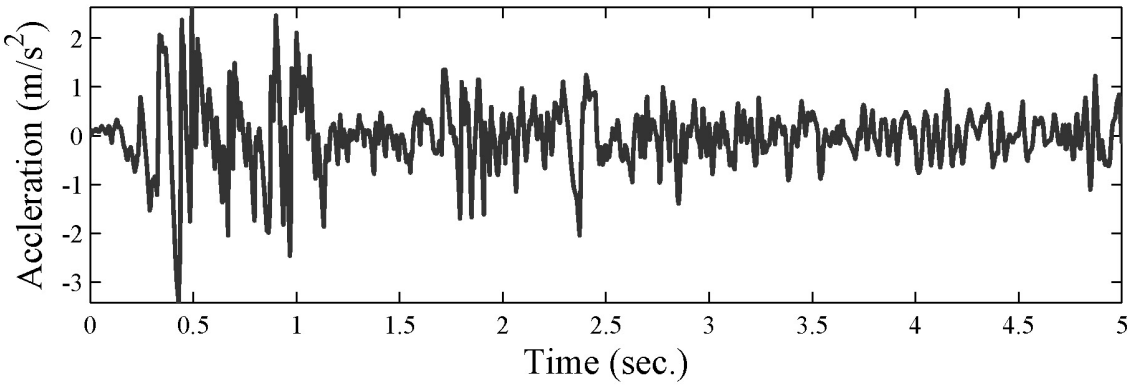

Figure 2-11. 1940 El Centro earthquake signal.

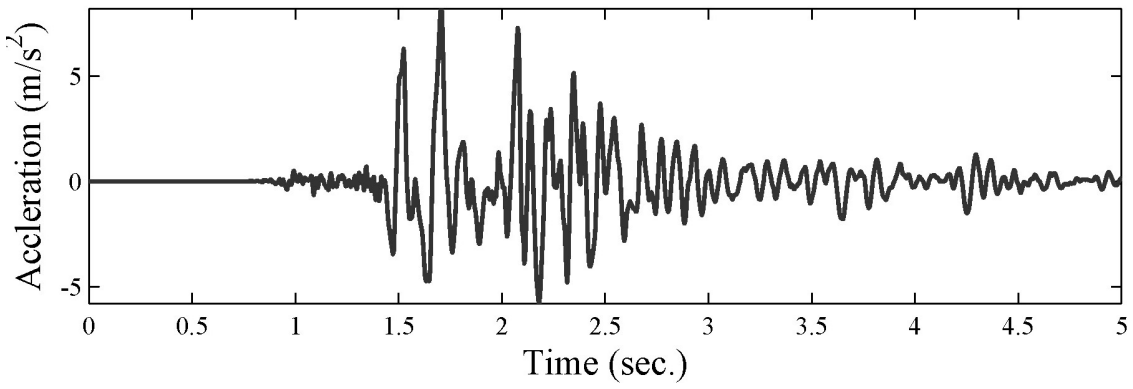

Figure 2-12. Kobe earthquake signal.

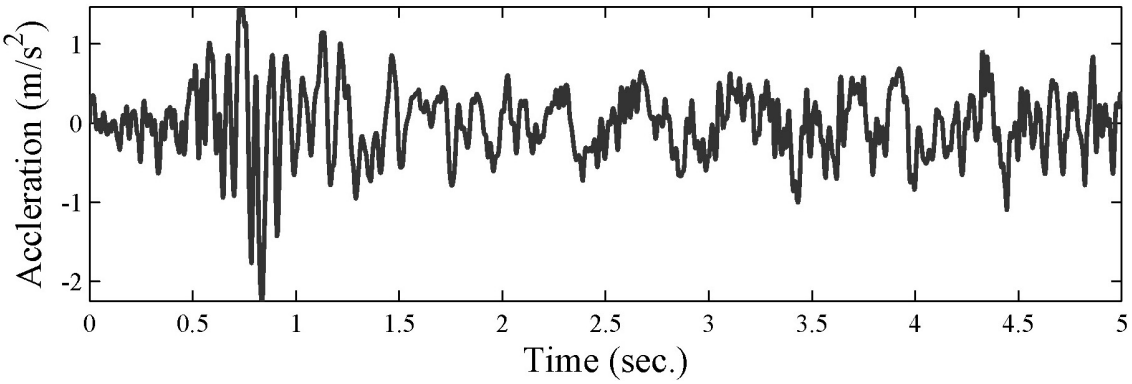

Figure 2-13. Hachinohe earthquake signal.

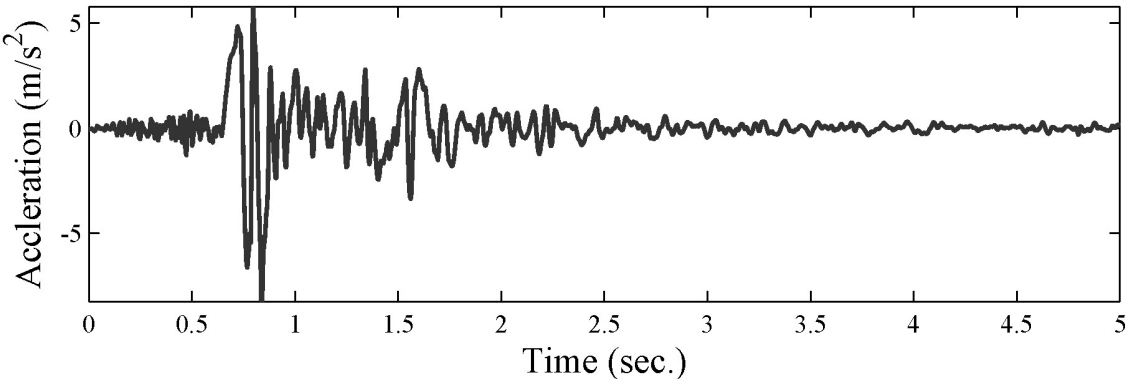

Figure 2-14. Northridge earthquake signal.

Figures 2-15 through 2-18 show comparisons of the actual accelerations at the third-story level and the predicted responses obtained from the PANFIS for the validating earthquakes. It is clear from the figures that the validated responses correlate well with the actual accelerations, meaning that the proposed PANFIS model is effective in modeling the nonlinear dynamic response to various earthquake signals. The accuracy of the identified model can be improved by increasing either the number of MFs or the step size. However, these increased parameters (i.e., overtraining) may not be an efficient approach for

validating the developed model using other data sets. Furthermore, it is not guaranteed that a larger number of MFs results in better performance of the PANFIS system (Mitchell *et al.* 2012).

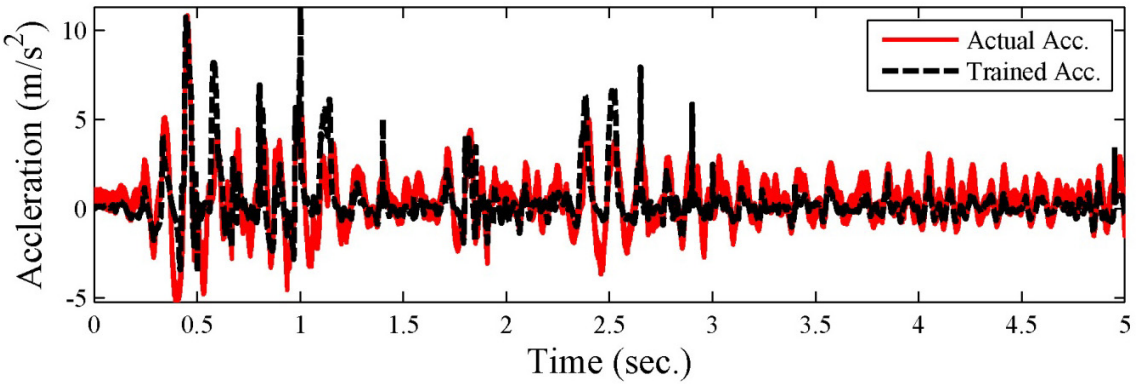

Figure 2-15. Validation: El Centro earthquake.

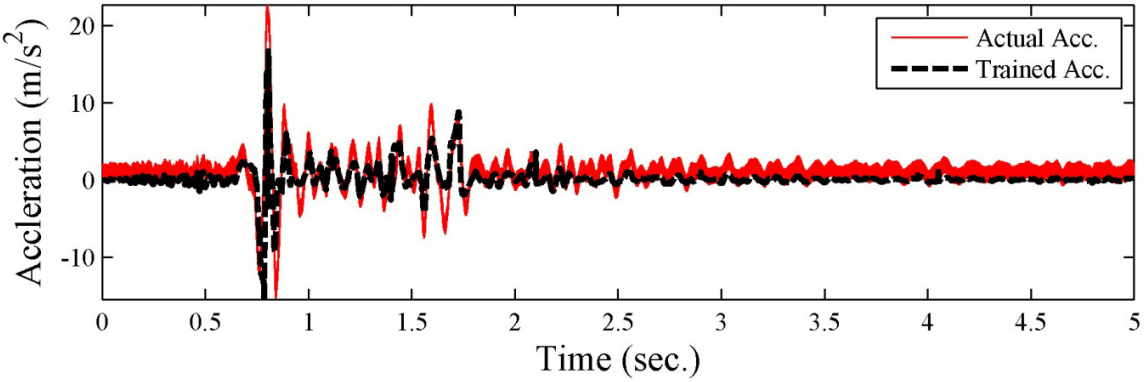

Figure 2-16. Validation: Northridge earthquake.

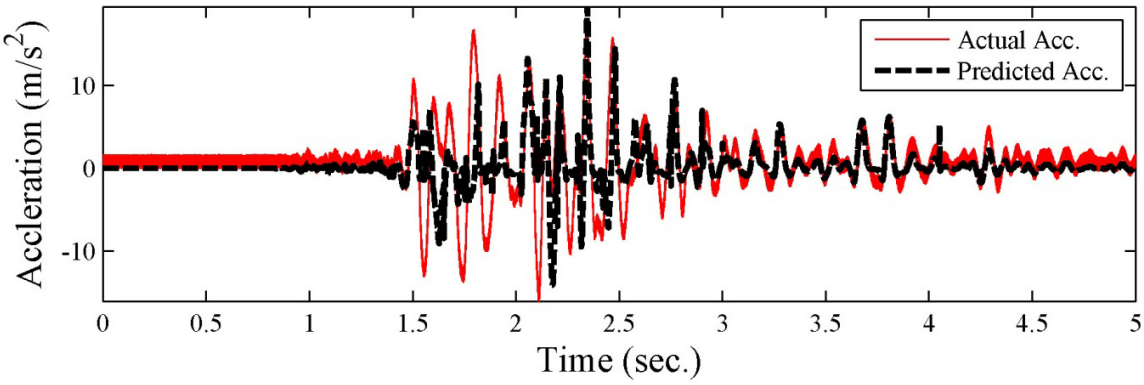

Figure 2-17. Validation: Kobe earthquake.

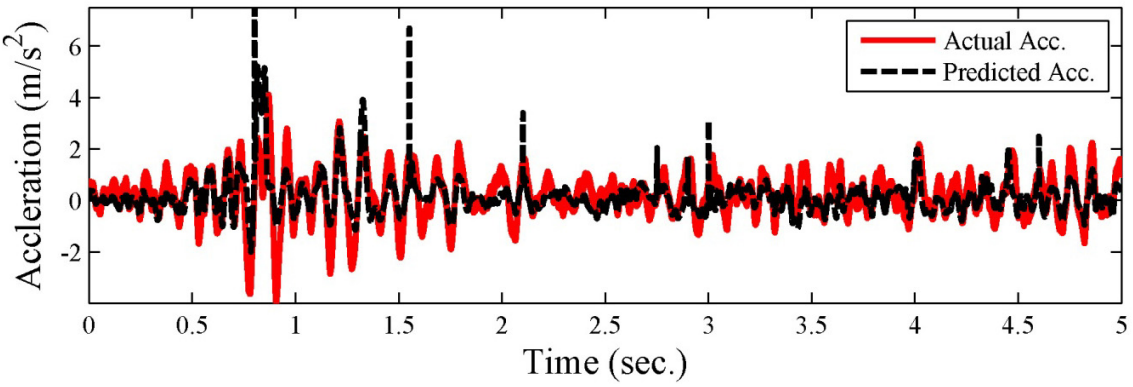

Figure 2-18. Validation: Hachinohe earthquake.

In order to quantify the error and the relationship between the predicted response and the actual response of the structure, six indices are introduced. The first index, J_1 is the maximum error of the estimated data.

$$J_1 = Max\left(\left|\hat{y} - \tilde{y}\right|\right), \tag{2-30}$$

where $\hat{y}$ is the estimation and $\tilde{y}$ is the actual structural response data. The next index, J_2 is the minimum error of the predicted data

$$J_2 = Min\left(\left|\hat{y} - \tilde{y}\right|\right). \tag{2-31}$$

Root-mean-square error (RMSE) index, J_3 is defined as

$$J_3 = RMSE = \sqrt{\frac{(\hat{y} - \tilde{y})^2}{N}} . \tag{2-32}$$

An index, J_4 is also used for evaluating the fitting rate of the predicted data as follows.

$$J_4 = \left(1 - \frac{\text{var}(|\hat{y} - \tilde{y}|)}{\text{var}(|\tilde{y}|)} \right). \tag{2-33}$$

Note that if the PANFIS model produces the same responses as the simulation model, the fitting rate J_4 would be 100%.

The training time is considered as another index J_5

$$J_5 \equiv \text{training time in minutes}, \tag{2-34}$$

which depends on the modeling method (ANFIS and PANFIS) and training data (the set of compressed artificial earthquake, control force and displacements) based on which the model is generated.

To compare the validation results of ANFIS and PANFIS, an index, J_6 is defined. It is simply the absolute value of the difference between the fitting rate index J_4 of the ANFIS and PANFIS results

$$J_6 = \left| J_4^{ANFIS} - J_4^{PANFIS} \right|. \tag{2-35}$$

The evaluations of the training results are provided in Table 2-1. It is evident form J_6 that the accuracy of the PANFIS model is close to that of ANFIS, while PANFIS's training time is 35.13% of ANFIS's, proving to be an efficient method.

Table 2-1. Training time and indices for ANFIS and PANFIS.

System	Number of MFs for each input	J_1 (m/s^2)	J_2 (m/s^2)	J_3 (m/s^2)	J_4 (%)	J_5 (min.)	J_6 (%)
ANFIS	2	16.78	0	2.973	73.22	2.068	1.68
PANFIS	2	16.87	1.131×10^{-5}	3.058	74.90	0.7265	

The validation errors are also provided in Table 2-2 for ANFIS and PANFIS models. It shows that the PANFIS model performs slightly better than ANFIS with a significant decrease in computation time (approximately 64.87% less than ANFIS).

Table 2-2. Validation of the trained ANFIS model.

Index	El Centro		Northridge		Kobe		Hachinohe	
	ANFIS	PANFIS	ANFIS	PANFIS	ANFIS	PANFIS	ANFIS	PANFIS
$J_1(\frac{m}{s^2})$	7.814	7.574	33.50	25.97	21.49	19.24	7.567	7.284
$J_2\ (10^{-7}\frac{m}{s^2})$	7.137	0.025	35.17	5.281	21.22	43.68	60.91	4.845
$J_3(\frac{m}{s^2})$	1.301	1.249	1.785	1.969	3.278	3.445	1.054	0.736
$J_4(\%)$	66.86	69.38	62.31	64.33	45.69	44.79	58.58	67.38
$J_6(\%)$	3.769		3.14		2.01		13.06	

2.4. Conclusion

In this chapter, an efficient PCA-based adaptive neuro-fuzzy inference system (PANFIS) is proposed for a fast nonlinear system identification of seismically excited building structures that are equipped with magnetorheological (MR) dampers. To fully exploit their advantages, Takagi-Sugeno fuzzy model, principal component analysis, and artificial neural networks are integrated to create the PANFIS system. The proposed model yields accurate results for the system identification of smart structures with significantly reduced time of computation compared to ANFIS. To train the input-output mapping function of the PANFIS model, an artificial earthquake signal and an MR damper force signal are used as a disturbance input signal and a control input, respectively, while the acceleration response is used as output data. Furthermore, a variety of earthquake records and their associated responses are used to validate the trained model. This approach can be applied to an integrated model of a building structure equipped with nonlinear MR devices without decoupling the identification procedure of the highly nonlinear MR damper from that of the primary building structure. It is demonstrated through the simulation results that the proposed PANFIS model is effective in identifying the nonlinear behavior of the seismically excited building-MR damper system while significantly decreasing the training time.

3. Dissipativity analysis of LQR controller applied to semi-active damping devices

3.1. Introduction

Semi-active dampers have attracted much attention in the field of structural control of various civil structures (Housner *et al.* 1997, Spencer *et al.* 1997, Symans *et al.* 1999, and Soong *et al.* 2002). These devices can be controlled to dissipate energy from structural systems subjected to external excitations, while actuators are designed to input energy to and dissipate energy from structural systems. Hence, it is important to analyze the dissipativity of the controller to implement an efficient semi-active control system into the structure. Dissipativity of the force produced by a smart damper can be expressed loosely by an inequality of the form $u_d v_d < 0$, where u_d is the damper force and v_d is the velocity at the point of action of the damper force. A control force can be defined as dissipative if it satisfies the inequality. The inequality describes the negative rate of injection of energy or equivalently, positive rate of dissipation of energy. Study on dissipativity of controllers designed for smart dampers helps evaluate or improve the performance of those controllers. Clipped optimal control strategy is commonly used for semi-acitve damping devices in structural control of civil structures. Therefore, the primary controller of this strategy is analyzed for dissipativity.

Clipped optimal control is one of the frequently used control strategies for the application of smart dampers to civil structural systems (Dyke *et al.* 1996, Dyke *et al.* 1998, Spencer *et al.* 2000, Erkus *et al.* 2002, Ramallo *et al.* 2002, and Johnson *et al.* 2006).

In this control strategy, the structure is assumed to behave linearly and a linear quadratic regulator (LQR) is considered as a primary controller, which is then clipped by a secondary controller if the control variable is not dissipative. Based on the dynamic model of the smart damper, a signal (e.g. voltage) is produced to induce the clipped control force in the damper (Figure 3-1). Note that in general, smart dampers are designed only to dissipate energy, therefore the controller needs to command dissipative forces.

The resulting controller, though effective in reducing structural responses, has not been proven to be optimal with respect to any criteria. Therefore, a definition of disspativity may be beneficial to evaluate or design a controller, which is consistent with the dissipative nature of smart dampers.

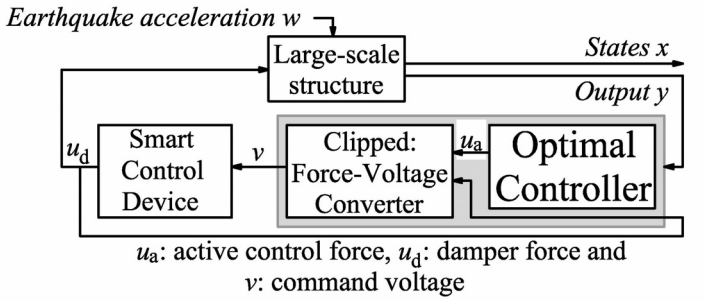

Figure 3-1. Architecture of the clipped optimal control strategy

A study of the literature suggests that the definition of dissipativity of the primary controller in a clipped optimal control strategy has not been extensively examined (Johnson *et al.* 2007). A stochastic index has been proposed by Inaudi (2000), $P[u_d v_d < 0]$, which helps estimate the probability of a control force being dissipative. This index, however, has not been generalized for integration into an optimal controller design.

Johnson *et al.* (2007) provides significant insight into dissipativity of LQR controllers, as it provides a deterministic definition for a dissipative force and proposes two generalized stochastic dissipativity indices defined based on dynamic time-history analyses. The generalized stochastic dissipativity indices proposed by Johnson *et al.* (2007) are not properly defined to be applied to the cases where the control variable is not a scalar, and also do not have a proper form to be used in a state-space formulation of the LQR design problem. Improved generalized definitions or indices are needed for deterministic evaluation of the dissipativity of controllers. These definitions or indices can also be used to integrate a deterministic dissipativity constraint into design of optimal controllers for smart dampers. This integration may pose a challenge due to nonlineaity of the constraint, which is addressed and investigated in this chapter.

There exists only two studies on integration of the disipativity of smart dampers with the optimal design of controllers for these devices (Johnson *et al.* 2000, Johnson *et al.* 2007). Johnson *et al.* (2007) implements a weak form of the energy dissipation rate ($u_d v_d$) in the objective function of a LQR control design problem resulting in minor improvements in performance. In another study, Johnson *et al.* (2007) proposes and integrates stochastic indices of dissipativity as constraints into a LQR control design problem. These stochastic indices are generalized to be appended to an eigenvalue problem (EVP) representation of an LQR problem in terms of linear matrix inequalities (LMIs). This problem is then analyzed numerically for specific cases. However, there is no deterministic analytical studies on dissipativity of controllers used for semi-active dampers applied to large civil structures.

In this chapter, a generalized deterministic definition of dissipativity is proposed for further analytical study. This generalization allows for appendage of a deterministic dissipativity constraint to LQR control design problem for analytical investigation. First-order conditions of optimality are then used to obtain an LQR optimal controller. The LQR controller is found to be optimal and dissipative with respect to the generalized deterministic form of dissipativity definition proposed. This result justifies the effectiveness of clipped optimal control for smart dampers with LQR as the primary controller.

3.2. Model definition

To design a LQR optimal controller for civil structural systems, the state-space formulation of dynamic behavior of civil structures may be required. The structure can be assumed to behave linearly. The smart damper forces can also be assumed as external forces. The smart damper's nonlinear behavior is not included in the model. The associated set of second-order ordinary differential equations of motion of the structure is given by

$$\mathbf{M}\ddot{\mathbf{x}} + \mathbf{C}\dot{\mathbf{x}} + \mathbf{K}\mathbf{x} = \mathbf{\Gamma}\mathbf{u} - \mathbf{\Lambda}\mathbf{w}, \tag{3-1}$$

where $\mathbf{w}$ denotes the disturbance signal which can be the forces due to the ground acceleration in seismic response problems or wind excitation forces; $\mathbf{M}$ is the mass matrix, $\mathbf{K}$ is the stiffness matrix, $\mathbf{C}$ is the damping matrix, and $\mathbf{x}$ is the vector of displacements of floors relative to the ground, $\dot{\mathbf{x}}$ is the velocity, $\ddot{\mathbf{x}}$ is the acceleration; and $\mathbf{\Gamma}$ and $\mathbf{\Lambda}$ are location vectors of control forces and disturbance signals, respectively. The set of second-

order ordinary differential equations as in Eq. (3-1) can be transformed into the state space model

$$\begin{aligned}\dot{\mathbf{z}} &= \mathbf{A}\mathbf{z} + \mathbf{B}\mathbf{u} + \mathbf{E}\mathbf{w} \\ \mathbf{y} &= \mathbf{C}\mathbf{z} + \mathbf{D}\mathbf{u} + \mathbf{H}\mathbf{n},\end{aligned} \tag{3-2}$$

where measurement noise is also taken into consideration. The parameters used in Eq. (3-2) are as follows

$$\mathbf{A} = \begin{bmatrix} \mathbf{0} & \mathbf{I} \\ -\mathbf{M}^{-1}\mathbf{K} & -\mathbf{M}^{-1}\mathbf{C} \end{bmatrix}, \tag{3-3}$$

$$\mathbf{B} = \begin{bmatrix} \mathbf{0} \\ \mathbf{M}^{-1}\mathbf{F} \end{bmatrix}, \tag{3-4}$$

$$\mathbf{C} = \begin{bmatrix} \mathbf{I} & \mathbf{0} \\ \mathbf{0} & \mathbf{I} \\ -\mathbf{M}^{-1}\mathbf{K} & -\mathbf{M}^{-1}\mathbf{C} \end{bmatrix}, \tag{3-5}$$

$$\mathbf{D} = \begin{bmatrix} \mathbf{0} \\ \mathbf{0} \\ \mathbf{M}^{-1}\mathbf{F} \end{bmatrix}, \tag{3-6}$$

$$\mathbf{E} = \begin{bmatrix} \mathbf{0} \\ \mathbf{L} \end{bmatrix}. \tag{3-7}$$

where $\mathbf{F}$ is the location vector of control elements such as dampers, actuators and etc., within the building structure, $\mathbf{n}$ is the measurement noise vector, $\mathbf{L}$ is a location matrix defined according to the disturbance considered, $\mathbf{H}$ is a location matrix defined appropriately for measurement noise, $\mathbf{z}$ and $\dot{\mathbf{z}}$ are the vector of displacements and the velocities of floor levels of the building structure, and $\mathbf{y}$ is the vector of outputs of the

structure.

This model is used to formulate a generalized deterministic definition of dissipativity of controllers used for semi-active dampers.

3.3. Dissipativity: definitions and indices

In this section, the definitions on dissipative forces are described in the context of civil engineering structural control problems.

3.3.1. *Strictly dissipative force*

3.3.1.1. *Definition*

A formal definition of a *strictly dissipative force* given by Johnson *et al.* (2007) is as follows. Consider a continuous external force $f(x,t)$, which is applied to a system on a surface region $x \in \Omega$. Let $v(x,t)$ be the velocity of the surface (with positive velocity in the same direction as positive forces). The *rate of energy added* to the system by the force $f(x,t)$ is given by

$$\frac{\partial E}{\partial t} = \int_{\Omega} f(x,t) v(x,t) d\Omega, \tag{3-8}$$

$f(x,t)$ is called a *strictly dissipative force* if the rate of energy added is negative for all $t \geq 0$. Or, without loss of generality,

$$\int_{\Omega} f(x,t)v(x,t)d\Omega \le \varepsilon(t) < 0 \text{ for all } t \ge 0 \Leftrightarrow f(x,t) \text{ is strictly dissipative}, \tag{3-9}$$

where $\varepsilon(t)$ is strictly negative. When the external force is a point load applied at point x_0 on the system, Eq. (3-9) can be simplified to

$$f(t)v(t) \le \varepsilon(t) < 0 \text{ for all } t \ge 0 \Leftrightarrow f(t) \text{ is strictly dissipative}, \tag{3-10}$$

where $v(t)$ is the velocity of point x_0, and the location parameter x_0 is dropped for simplicity. The definition given in Eq. (3-10) is more suitable for a civil engineering control problem, since the control force can generally be modelled as a point load. This condition simply states a necessary and sufficient condition. The force is dissipative if and only if the direction of the force and the velocity are opposite.

3.3.1.2. *Example*

A familiar example to illustrate this condition might be a simple dashpot element which provides a force f_c proportional to the relative velocity of the two ends of the damper $v_d(t)$ such as

$$f_c = -cv_d(t), \tag{3-11}$$

where $c > 0$ is the damping coefficient. Using Eq. (3-11), the definition given in Eq. (3-10) results in

$$f_c v_d(t) = -cv_d^2(t), \tag{3-12}$$

which is always less than or equal to zero and proves that the force provided by the damper in this example is dissipative as defined in Eq. (3-10).

3.3.1.3. *Proposed definition*

Since state-space models are commonly used in the context of structural control, a generalized state-space formulation for the dissipativity condition given in Eq. (3-10) is proposed. In the state-space model (3-2), the control force acting on states of the structure model is given by $\mathbf{Bu}$, therefore the Eq. (3-10) can be generalized as follows

$$\left(\mathbf{Bu}\right)^T \mathbf{Gz} \le \varepsilon\left(t\right) < 0, \tag{3-13}$$

where $\varepsilon\left(t\right)$ is strictly negative and $\mathbf{G}$ is a positive semi-definite matrix appropriately chosen to define (strict) dissipativity condition for control forces. A common practice is to use displacement or drift responses as the first set of variables in state vector $\mathbf{z}$ and velocities as the second set of variables in state vector. Therefore, defining matrix $\mathbf{G}$ as

$$\mathbf{G} = \begin{bmatrix} \mathbf{0} & \mathbf{0} \\ \mathbf{0} & \mathbf{g} \end{bmatrix}, \tag{3-14}$$

results in a set of equations, each in the form of Eq. (3-10). The matrix $\mathbf{g}$ is positive-definite. The number of columns of $\mathbf{g}$ is equal to the number of states with respect to which the control forces are defined to be dissipative.

3.3.2. *Time index for dissipative control forces*

To calculate the percentage of time that the primary controller is commanding dissipative forces, Johnson *et al.* (2007) defines a time index

$$D_{\%} = 1 - \frac{1}{T}\int_0^T H\left[u_a v_d\right] dt \,,\; D_{\%} \in [0,1], \tag{3-15}$$

where $H(\cdot)$ is the Heaviside unit step function defined as follows

$$H(s) = \begin{cases} 1 & s \geq 0 \\ 0 & s < 0 \end{cases}, \tag{3-16}$$

T is the total time during which the controller is commanding control forces, u_a is the control force, and v_d is the velocity at the point of action of the damper force. According to this definition, higher values of $D_{\%}$ implies more dissipativity of u_a.

3.3.3. *Probability of dissipativity of the control force*

For a linear system with stationary Gaussian response, Inaudi (2000) gives the probability that the control force is strictly dissipative as

$$D_p = P\left(u_a v_d < 0\right) = \frac{\operatorname{acos}(\rho)}{\pi},\; D_p \in [0,1], \tag{3-17}$$

where $\operatorname{acos}(\cdot)$ is the inverse cosine function, ρ is the correlation coefficient between u_a and v_d. Values of D_p higher than or equal to 50% implies dissipative characteristic of u_a.

3.3.4. *Expected value of the energy flow rate*

The dissipative force conditions given by Eq. (3-10) and (3-13) are deterministic. Stochastic definitions can also be given for dissipativity of control forces. The expected value of Eq. (3-10) is proposed by Johnson *et al.* (2007) to be used to define the dissipativity of the primary control force as follows

$$u_a(t) \text{ is strictly dissipative} \Rightarrow E\left[u_a(t) v_d(t)\right] \le E\left[\varepsilon(t)\right] = \mu_\varepsilon(t) < 0, \tag{3-18}$$

where $E[\cdot]$ is the expected value operator and $\mu_\varepsilon(t)$ is strictly negative. Generalized form of Eq. (3-18) as developed in this chapter is given as

$$\mathbf{u}(t) \text{ is strictly dissipative} \Rightarrow E\left[\left(\mathbf{Bu}\right)^T \mathbf{Gz}\right] \le E\left[\boldsymbol{\varepsilon}(t)\right] = \boldsymbol{\mu}_\varepsilon(t) < \mathbf{0}, \tag{3-19}$$

It should be noted that the conditions stated in Eq. (3-18) and (3-19) are necessary but not sufficient conditions for dissipativity of the control force and lower value of $\mu_\varepsilon(t)$ only imply that the control force is dissipating more energy. Another index is proposed by Johnson *et al.* (2007) as

$$D_e = E\left[u_a v_d\right], \tag{3-20}$$

called the *mean energy flow rate,* and is normalized as follows

$$D_{ne} = \frac{E\left[u_a v_d\right]}{\sqrt{E\left[u_a^2\right]}\sqrt{E\left[v_d^2\right]}}. \tag{3-21}$$

where D_{ne} is called the *normalized mean energy flow rate*. Negative-definiteness of D_e and D_{ne} provide necessary but not sufficient conditions for dissipativity of the control force.

In this section, the relevant definitions and indices were reviewed. In the next section, the dissipative LQR optimal control problem is examined.

3.4. Dissipative LQR optimal control problem

Before analyzing the dissipativity of the LQR controller, a typical LQR optimal control problem is examined.

3.4.1. *LQR optimal control problem*

LQR is frequently used in the field of structural control of buildings and/or bridges for an efficient performance. Thus, LQR is assumed to be the primary controller strategy in this chapter. The LTI system as in Eq. (3-2) is considered without the disturbance and measurement noise

$$\begin{aligned} \dot{\mathbf{z}} &= \mathbf{A}\mathbf{z} + \mathbf{B}\mathbf{u} \\ \mathbf{y} &= \mathbf{C}\mathbf{z} + \mathbf{D}\mathbf{u} \end{aligned}, \tag{3-22}$$

where $\mathbf{z}$ is the state vector, $\mathbf{u}$ is the control vector, (here, the vector of control forces) and $\mathbf{y}$ is the vector of outputs of the system. The goal is to find control variable $\mathbf{u}$, which satisfies the optimization problem

$$\min_{\mathbf{u}} \left\{ \frac{1}{2} \int \left(\mathbf{z}^T \mathbf{Q} \mathbf{z} + \mathbf{u}^T \mathbf{R} \mathbf{u} \right) dt \right\}, \tag{3-23}$$

$$\text{subject to Eq.}(3\text{-}22)$$

where $\mathbf{Q} = \mathbf{Q}^T \geq 0$, and $\mathbf{R} = \mathbf{R}^T > 0$ are weighting matrices. The design parameters should satisfy the following inequalities for the problem defined by Eq. (3-22) and (3-23) to be well posed

$$\mathbf{W} = \begin{bmatrix} \mathbf{Q} & \mathbf{0} \\ \mathbf{0} & \mathbf{R} \end{bmatrix} \geq \mathbf{0}. \tag{3-24}$$

The Hamiltonian for this problem can be defined as

$$H = \frac{1}{2}\mathbf{z}^T\mathbf{Q}\mathbf{z} + \frac{1}{2}\mathbf{u}^T\mathbf{R}\mathbf{u} + \boldsymbol{\lambda}^T\left(\mathbf{A}\mathbf{z} + \mathbf{B}\mathbf{u}\right), \tag{3-25}$$

where $\boldsymbol{\lambda}$ is the vector of costate variables and has the same dimension as the state vector. Optimal states and costates are derived from the following necessary conditions given by Geering (2007) as

$$\dot{\mathbf{z}}^* = \nabla_{\lambda} H\,, \tag{3-26}$$

$$\dot{\boldsymbol{\lambda}}^* = -\nabla_{\mathbf{z}} H\,, \tag{3-27}$$

$$\frac{\partial H}{\partial \mathbf{u}^*} = 0\,. \tag{3-28}$$

where * denotes optimality. Assuming

$$\boldsymbol{\lambda}^* = \mathbf{K}\mathbf{z}^*, \tag{3-29}$$

and substituting for Hamiltonian in Eq. (3-28) results in

$$\mathbf{u}^* = -\mathbf{R}^{-1}\mathbf{B}^T\mathbf{K}\mathbf{z}^*. \tag{3-30}$$

Equations (3-26), (3-27), and (3-30) lead to the following Riccati differential equation

$$\dot{\mathbf{K}} + \mathbf{A}^T\mathbf{K} + \mathbf{K}\mathbf{A} - \mathbf{K}\mathbf{B}\mathbf{R}^{-1}\mathbf{B}^T\mathbf{K} + \mathbf{Q} = \mathbf{0}\,, \tag{3-31}$$

from which the control gain $\mathbf{K}$ is obtained. It should be noted that since the objective function is quadratic and the constraint is affine, the necessary conditions stated in Eq. (3-26)-(3-28) are also sufficient.

In following sections, a review of a specific optimal control problem is provided. The results of this problem are used to investigate the dissipative LQR optimal control problem. To investigate the dissipativity of the LQR controller, LQR optimal control problem is defined subject to the system dynamics equality constraint as in Eq. (3-22) and the controller dissipativity inequality constraint as in Eq. (3-13), and then the optimal controller is obtained. The objective function is convex. The system dynamics constraint is affine and assuming Eq. (3-29) is satisfied, the dissipativity constraint can also be convex. Therefore, conditions provided are necessary and sufficient conditions of optimality. The controller can then be verified to be dissipative according to condition stated in Eq. (3-13).

3.4.2. *Optimal control problem* Σ *with state constraint*

A review of a specific optimal control problem is given in this section and the first-order necessary conditions for optimality of this problem are given in the next section. It is desired to minimize the following cost functional

$$\min_{\mathbf{u}}\left\{\int L\left(\mathbf{x}(t),\mathbf{u}(t),t\right)dt\right\}, \tag{3-32}$$

subject to system dynamics constraint

$$\dot{\mathbf{z}} = \mathbf{f}\left(\mathbf{x}(t),\mathbf{u}(t),t\right), \tag{3-33}$$

and inequality constraint

$$\mathbf{g}(\mathbf{x},t) \le \mathbf{0}. \tag{3-34}$$

3.4.3. *First-order necessary optimality conditions for problem* Σ

In this section, first-order necessary conditions for optimality of problem Σ are provided. A more detailed analysis of this problem can be found in Geering (2007).

Two cases are considered for this problem. The inequality constraint can be active during a specific time interval, which is considered as case I and inactive for the rest of the time, considered as case II. The first-order necessary conditions for optimality for case I are as follows

$$\dot{\mathbf{z}}^* = \nabla_{\boldsymbol{\lambda}} H\ , \tag{3-35}$$

$$\dot{\boldsymbol{\lambda}}^* = -\nabla_{\mathbf{z}} H - \left(\mu_l^*\right)^T \nabla_{\mathbf{z}} \mathbf{g}^{(l)}, \tag{3-36}$$

$$\frac{\partial \bar{H}}{\partial \mathbf{u}^*} = 0, \bar{H} = H + \left(\mu_l^*\right)^T \mathbf{g}^{(l)}, \tag{3-37}$$

$$\mu_l^* \ge 0\ , \tag{3-38}$$

$$\mathbf{g} = \mathbf{0}, \mathbf{g}^{(l)} = \mathbf{0}\ . \tag{3-39}$$

The first-order necessary conditions for optimality for case II are as follows

$$\dot{\mathbf{z}}^* = \nabla_{\lambda} H \,, \tag{3-40}$$

$$\dot{\boldsymbol{\lambda}}^* = -\nabla_{\mathbf{z}} H \,, \tag{3-41}$$

$$\frac{\partial H}{\partial \mathbf{u}^*} = 0 \,, \mathbf{g} < \mathbf{0} \tag{3-42}$$

$$\mathbf{g} < \mathbf{0}, \tag{3-43}$$

where

$$H = L\left(\mathbf{x}(t), \mathbf{u}(t), t\right) + \boldsymbol{\lambda}^T \mathbf{f}\left(\mathbf{x}(t), \mathbf{u}(t), t\right), \tag{3-44}$$

and $\mathbf{g}^{(l)}$ is the l^{th} time derivative of the constraint $\mathbf{g}$, in which $\mathbf{u}$ appears explicitly. Scalar μ_l is the corresponding costate variable.

3.4.4. *Dissipative LQR optimal control problem*

In this section, the dissipative LQR optimal control problem is introduced and using the results of section 3.4.3., the commonly used LQR control variable is found to be dissipative.

The dissipative LQR optimal control problem is defined as follows: Find control variable $\mathbf{u}$, which satisfies the optimization problem

$$\min_{\mathbf{u}} \left\{ \frac{1}{2} \int \left(\mathbf{z}^T \mathbf{Q} \mathbf{z} + \mathbf{u}^T \mathbf{R} \mathbf{u} \right) dt \right\}. \tag{3-45}$$

subject to $(3\text{-}13)$, and $(3\text{-}22)$

It is assumed that $\varepsilon(t)=0$ in the dissipativity inequality constraint. Due to specific properties of the inequality constraint, case I in this problem is found to be equivalent to case II. Therefore, only case I is examined in detail.

3.4.4.1. *Dissipativity constraint active*

Condition stated in Eq. (3-35) yields

$$\dot{\mathbf{z}}^* = \mathbf{A}\mathbf{z}^* + \mathbf{B}\mathbf{u}\,. \tag{3-46}$$

The control variable $\mathbf{u}$ appears explicitly in the inequality constraint $\mathbf{g} = (\mathbf{B}\mathbf{u})^T \mathbf{G}\mathbf{z}$, therefore

$$\mathbf{g}^l = (\mathbf{B}\mathbf{u})^T \mathbf{G}\mathbf{z}\,, \tag{3-47}$$

according to which

$$\nabla_{\mathbf{z}}\mathbf{g}^{(l)} = \mathbf{G}^T\mathbf{B}\mathbf{u}\,. \tag{3-48}$$

Therefore, conditions states in Eq. (3-36) and (3-37) result in

$$\dot{\boldsymbol{\lambda}}^* + \mathbf{A}^T\boldsymbol{\lambda}^* + \mathbf{Q}\mathbf{z}^* + \mu^*\mathbf{G}^T\mathbf{B}\mathbf{u}^* = \mathbf{0}\,, \tag{3-49}$$

$$\mathbf{R}\mathbf{u}^* + \mathbf{B}^T\boldsymbol{\lambda}^* + \mu^*\mathbf{B}^T\mathbf{G}\mathbf{z}^* = \mathbf{0}\,. \tag{3-50}$$

Using Eq. (3-39), Eq. (3-49) and (3-50) can be simplified. Assuming $\mathbf{z}^* \neq \mathbf{0}$, transposing both sides of (3-49) and multiplying both sides of (3-49) by $\mathbf{z}^*$ yields

$$\left(\dot{\boldsymbol{\lambda}}^*\right)^T \mathbf{z}^* + \left(\boldsymbol{\lambda}^*\right)^T \mathbf{A}\mathbf{z}^* + \left(\mathbf{z}^*\right)^T \mathbf{Q}^T \mathbf{z}^* + \mu^* \left(\mathbf{B}\mathbf{u}^*\right)^T \mathbf{G}\mathbf{z}^* = \mathbf{0}. \tag{3-51}$$

Equation (44) has to hold irrespective of the initial state at all times, which along with Eq. (39) lead to

$$\dot{\boldsymbol{\lambda}}^* + \mathbf{A}^T \boldsymbol{\lambda}^* + \mathbf{Q}\mathbf{z}^* = \mathbf{0}. \tag{3-52}$$

Therefore, conditions (3-36) and (3-41) are equivalent. Based on condition (3-39), Eq. (3-37) and (3-42) are also equivalent. Therefore, following conditions are to hold for both cases I and II considered for the problem.

$$\dot{\mathbf{z}}^* = \mathbf{A}\mathbf{z}^* + \mathbf{B}\mathbf{u}, \tag{3-53}$$

$$\dot{\boldsymbol{\lambda}}^* + \mathbf{A}^T \boldsymbol{\lambda}^* + \mathbf{Q}\mathbf{z}^* = \mathbf{0}, \tag{3-54}$$

$$\mathbf{R}\mathbf{u}^* + \mathbf{B}^T \boldsymbol{\lambda}^* = \mathbf{0}, \tag{3-55}$$

which were derived in section 4.1. for LQR optimal control problem. Same process as in section 4.1. yields the following controller

$$\mathbf{u}^* = -\mathbf{R}^{-1}\mathbf{B}^T \mathbf{K}\mathbf{z}^*. \tag{3-56}$$

Using dissipativity constraint states in Eq. (3-13), control variable (3-49) and assuming $\varepsilon = 0$, the left-hand side of the dissipativity constraint becomes

$$\left(\mathbf{Bu}\right)^T \mathbf{Gz} = -\mathbf{z}^T \mathbf{KBR}^{-1}\mathbf{B}^T \mathbf{Gz}, \tag{3-57}$$

which is examined if it is a negative semi-definite matrix. The solution to the Riccati differential equation is positive semi-definite

$$\mathbf{K} \geq \mathbf{0}. \tag{3-58}$$

One of the conditions for well-posedness of the LQR problem is for the weighting matrix $\mathbf{R}$ to be positive definite. Matrix $\mathbf{BB}^T$ is also positive semi-definite and matrix $\mathbf{G}$ can only be defined meaningful if defined positive semi-definite. Therefore the matrix in Eq. (3-50) is a negative semi-definite matrix which implies the LQR controller is dissipative with respect to the definition of dissipativity as in Eq. (3-13).

3.6. Numerical example

3.6.1. *Model Parameters*

The model investigated in this chapter is an eight-story building (Yang 1982), with the following parameters

$$\mathbf{M} = 345,600\mathbf{I}_{8\times 8}\ \text{kg}, \tag{3-59}$$

$$\mathbf{K} = 340,400\begin{bmatrix} 2 & -1 & 0 & \cdots \\ -1 & 2 & \ddots & 0 \\ 0 & \ddots & 2 & -1 \\ \cdots & 0 & -1 & 1 \end{bmatrix}_{8\times 8} \frac{\text{kN}}{\text{m}}, \tag{3-60}$$

$$\mathbf{C} = 2,937,000\begin{bmatrix} 2 & -1 & 0 & \cdots \\ -1 & 2 & \ddots & 0 \\ 0 & \ddots & 2 & -1 \\ \cdots & 0 & -1 & 1 \end{bmatrix}_{8\times 8} \frac{\text{Ns}}{\text{m}}, \tag{3-61}$$

$$\mathbf{F} = \begin{bmatrix} \mathbf{0}_{1\times 15} & 1 \end{bmatrix}^T, \tag{3-62}$$

$$\mathbf{L} = \mathbf{I}_{8\times 8}, \tag{3-63}$$

$$\mathbf{H} = \mathbf{I}_{16\times 16}. \tag{3-64}$$

The $\mathbf{Q}$ matrix for LQR optimal control design is defined as a diagonal one with the following elements

$$\mathbf{q} = 10^{-12}\begin{bmatrix} 10^{-4}\mathbf{1}_{7\times 1} & 10^{-2} & 10^{-15} & 10^{-2}\mathbf{1}_{7\times 1} & 1 & 10^{-15} \end{bmatrix}. \tag{3-65}$$

3.6.2. *Evaluation indices*

The indices for evaluation of the control performance are as follows

$$J_1 = D_{\%}, \tag{3-66}$$

as defined in Eq. (3-15).

$$J_2 = D_p, \tag{3-67}$$

defined in Eq. (3-17).

Mean energy flow rate as in Eq. (3-19) is also used

$$J_3 = D_e = E\left[(\mathbf{Bu})^T \mathbf{Gz}\right], \tag{3-68}$$

and normalized as in Eq. (3-21)

$$J_4 = D_{ne}. \tag{3-69}$$

To investigate how strict the dissipativity constraint is, another normalized index is defined as

$$J_5 = \frac{Max\left((\mathbf{Bu})^T \mathbf{Gz}\right)}{Max\left(\left|(\mathbf{Bu})^T \mathbf{Gz}\right|\right)}. \tag{3-70}$$

where $|\cdot|$ is the absolute value operator. If the controller produces significant actuating force at any time during simluation, this index will have a value of one. Otherwise, it will have a value less than one.

The ratio of the total dissipated energy to the total input energy is

$$J_6 = \frac{\int\left[(\mathbf{Bu})^T \mathbf{Gz}\, H\left(-(\mathbf{Bu})^T \mathbf{Gz}\right)\right]dt}{\int\left|(\mathbf{Bu})^T \mathbf{Gz}\right|dt}, \tag{3-71}$$

The ratio of the root-mean-square (RMS) of the total dissipated energy over the RMS of the total input energy is

$$J_7 = \frac{\left(\int_0^T\left[(\mathbf{Bu})^T \mathbf{Gz}\, H\left(-(\mathbf{Bu})^T \mathbf{Gz}\right)\right]^2 dt\right)^{1/2}}{\left(\int_0^T\left((\mathbf{Bu})^T \mathbf{Gz}\right)^2 dt\right)^{1/2}}, \tag{3-72}$$

Following indices are also defined to evaluate the ratio of controlled over

uncontrolled responses of the structure.

$$J_8 = \frac{\text{Max}\left(\left|z_8^c\right|\right)}{\text{Max}\left(\left|z_8^u\right|\right)}, \tag{3-73}$$

$$J_9 = \frac{\text{Mean}\left(\left|z_8^c\right|\right)}{\text{Mean}\left(\left|z_8^u\right|\right)}, \tag{3-74}$$

$$J_{10} = \frac{\text{Max}\left(\left|\ddot{z}_8^c\right|\right)}{\text{Max}\left(\left|\ddot{z}_8^u\right|\right)}, \tag{3-75}$$

$$J_{11} = \frac{\text{Mean}\left(\left|\ddot{z}_8^c\right|\right)}{\text{Mean}\left(\left|\ddot{z}_8^u\right|\right)}. \tag{3-76}$$

where z_8 and $\ddot{z}_8$ are the displacement and acceleration of the eighth story level, respectively.

Since drift is an important variable in the design of structures, J_{12} and J_{13} are defined as the maximum and mean drift of all the floors

$$J_{12} = \text{Max}\left(\left|z_{i+1} - z_i\right|\right),\ i = 1, 2, \ldots, 7. \tag{3-77}$$

$$J_{13} = \text{Mean}\left(\left|z_{i+1} - z_i\right|\right),\ i = 1, 2, \ldots, 7. \tag{3-78}$$

A summary of the simulation results is presented in Table 3-1. As discussed in sections 3.3.2., higher values of J_1 close to 100% imply higher dissipativity of the control force. As observed form Table 3-1, LQR proves to produce a more dissipative force compared to PID control method.

In section 3.3.3., it was mentioned that values of J_2 higher than 50% indicates the

dissipative characteristic of the control force. According to Table 3-1., LQR method proves to be dissipative according to index defined in section 3.3.3., whereas PID method proves not to be dissipative.

Index J_3, defined in section 3.3.4., gives the mean value of the input energy to the structures. Results in Table 3-1. suggest that the mean input energy produced by PID control method is positive, thus proving it to actuating rather than dissipating. Normalizing index J_3 gives index J_4, which implies the dissipativity of LQR and proves PID contorl method to be actuating.

A control variable satisfying Eq. (3-13) results in a normalized J_5 index less than or equal to zero. On the other hand, control variable producing large actuating forces results in a J_5 index of one. Comparing values of J_5 for LQR and PID shows how PID is actuating the structure compared to LQR.

Values of normalized indices J_6 and J_7 closer to one imply higher dissipativity of the LQR controller compared to PID contorller as observed from Table 3-1.

Both LQR and PID control methods show comparable performances in reducing the structural responses as observed from indices J_8 through J_{13} with LQR performing slightly better in 80% of the cases.

Table 3-1. Summary of indices for uncontrolled, LQR controlled and PID controlled responses.

Index	Control method	Excitation			
		El Centro	Kobe	Hachinohe	Northridge
J_1(%)	LQR	84.33	82.09	84.7	84.2
	PID	39.99	40.72	38.72	40.65
J_2 (%)	LQR	61.71	62.8	62.78	63.57
	PID	37.86	37.93	35.78	35.59
J_3	LQR	-0.044	-0.322	-0.044	-0.142
	PID	0.5534	3.491	0.2336	1.063
J_4	LQR	-0.3597	-0.3913	-0.3909	-0.4135
	PID	0.3722	0.3702	0.4321	0.4375
J_5	LQR	0.0452	0.0282	0.1019	0.0462
	PID	1	1	1	1
J_6	LQR	-0.9840	-0.9873	-0.9826	-0.9853
	PID	-0.2753	-0.2635	-0.2553	-0.2798
J_7	LQR	0.999	0.9994	0.9979	0.9990
	PID	0.2054	0.1663	0.1448	0.1869
J_8	LQR	**0.2167**	**0.2246**	**0.2929**	0.4191
	PID	0.2438	0.3555	0.3278	**0.3114**
J_9	LQR	**0.1659**	**0.1787**	0.1899	0.1461
	PID	0.1692	0.2197	**0.1434**	**0.1218**
J_{10}	LQR	**0.3414**	**0.3860**	**0.3752**	**0.4726**
	PID	0.4120	0.5660	0.4287	0.5345
J_{11}	LQR	**0.2688**	**0.3407**	**0.2033**	**0.2078**
	PID	0.3477	0.4161	0.2224	0.2350
J_{12}	LQR	**0.0115**	**0.0328**	**0.0094**	0.0415
	PID	0.0148	0.0512	0.0125	**0.0361**
J_{13}	LQR	**0.0012**	**0.0018**	**0.0020**	**0.0014**
	PID	0.0021	0.0037	**0.0020**	0.0023

3.6.3. *Time-history results*

Figures 3-2 and 3-3 show the effectiveness of LQR and PID controllers in

decreasing maximum displacements and maximum accelerations at different floor levels for four different earthquakes. LQR controller performs slightly better than PID in all cases. Favorable performance of LQR controller is theoretically guaranteed, since LQR was proved to minimize the quadratic cost functional in (3-23) and (3-25). This can be observed from Figures 3-2 and 3-3, where LQR demonstrates consistent favorable performance for different earthquakes. Favorable performance coupled with dissipativity justifies the wide use of LQR as primary controller for clipped optimal control strategy.

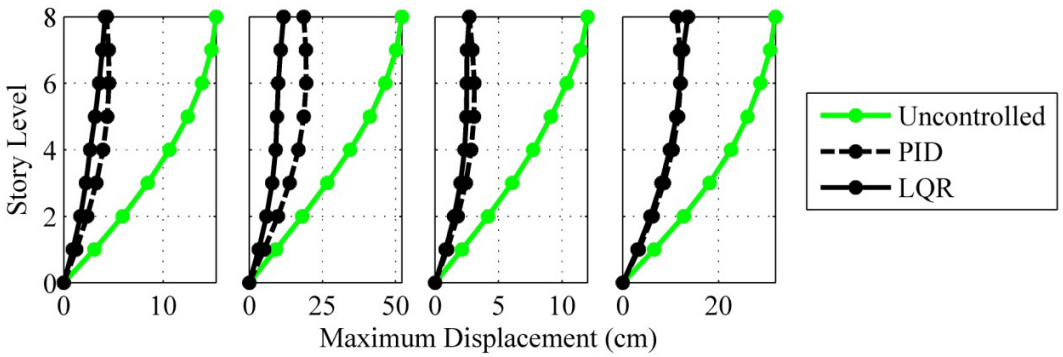

Figure 3-2. Maximum displacement for each story for different earthquakes (from left to right: El Centro, Kobe, Hachinohe and Northridge earthquakes).

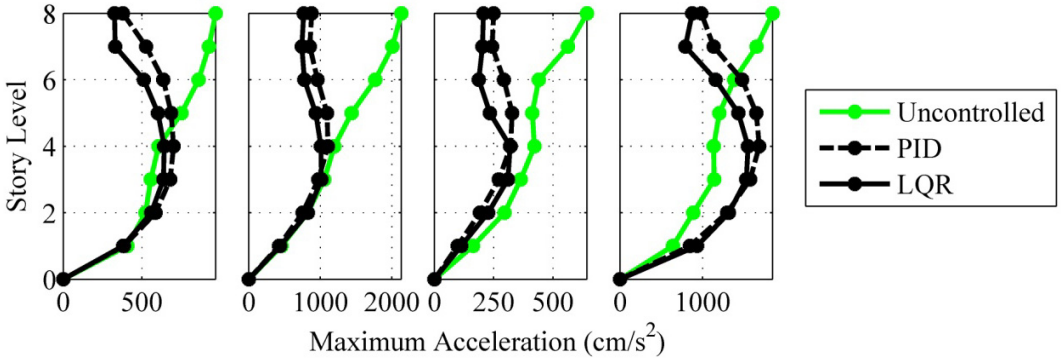

Figure 3-3. Maximum acceleration for each story for different earthquakes (from left to right: El Centro, Kobe, Hachinohe and Northridge earthquakes).

Figures 3-4, 3-5, 3-6, and 3-7 show the time-history of uncontrolled, LQR, and PID controlled displacements at top floor level of the eight story building. The LQR controller shows better performance with dissipativity compared to PID controller as quantified in Table 3-1. and illustrated in following figures.

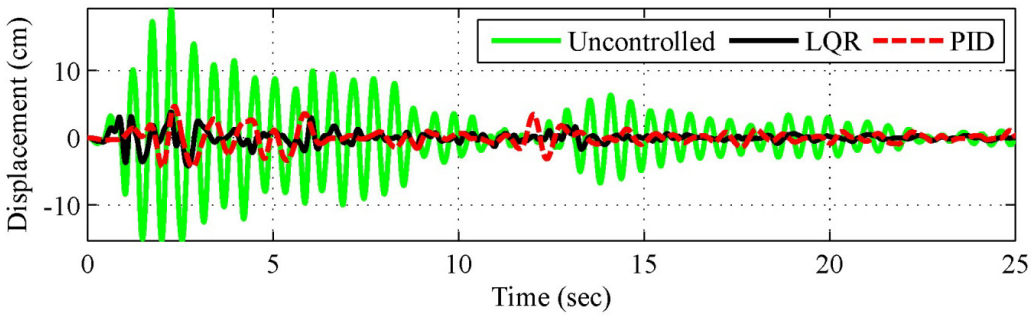

Figure 3-4. Comparision of displacements at the top floor level: El Centro earthquake.

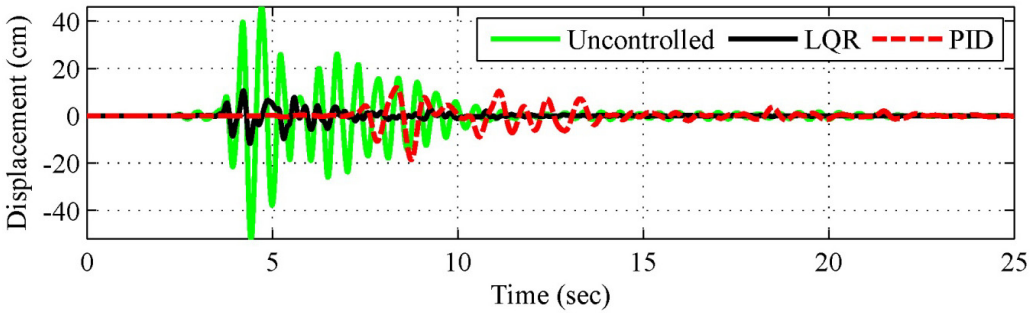

Figure 3-5. Comparision of displacements at the top floor level: Kobe earthquake.

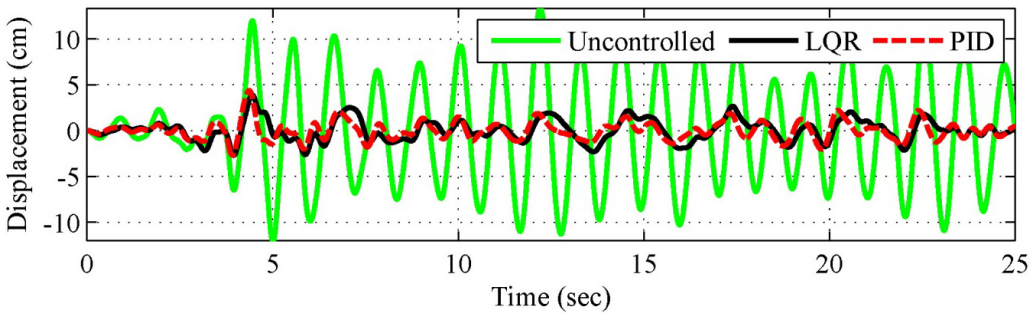

Figure 3-6. Comparision of displacements at the top floor level: Hachinohe earthquake.

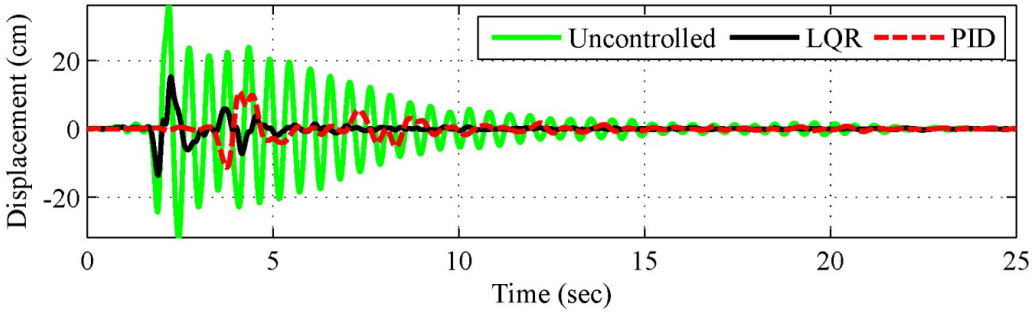

Figure 3-7. Comparision of displacements at the top floor level: Northridge earthquake.

Figures 3-8 through 3-11 demonstrate the time-history of the generalized deterministic

dissipativity constraint defined in Eq. (3-13). Negative values of $(\mathbf{Bu})^T \mathbf{Gz}$ imply the dissipativity of the controller. Figures 3-8 through 3-11 illustrate the dissipativity of the LQR controller and very low dissipativity of the PID controller during the simulation.

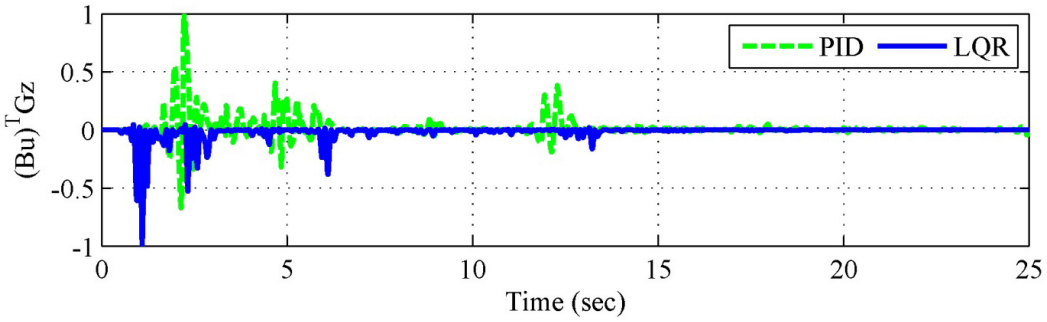

Figure 3-8. Time-history of the dissipativity constraint: El Centro earthquake.

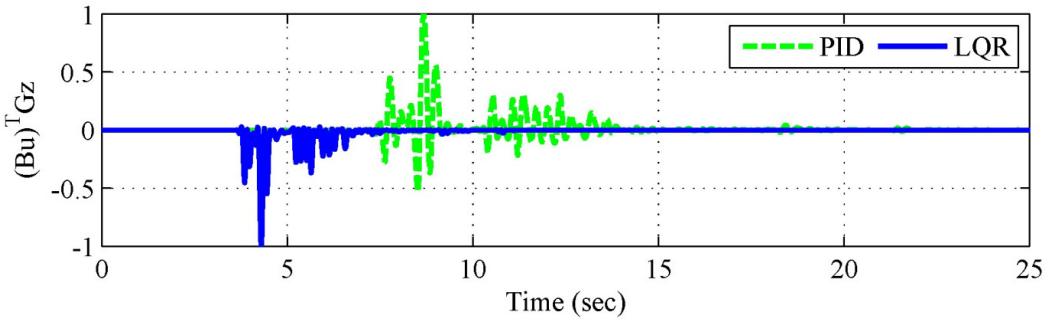

Figure 3-9. Time-history of the dissipativity constraint: Kobe earthquake.

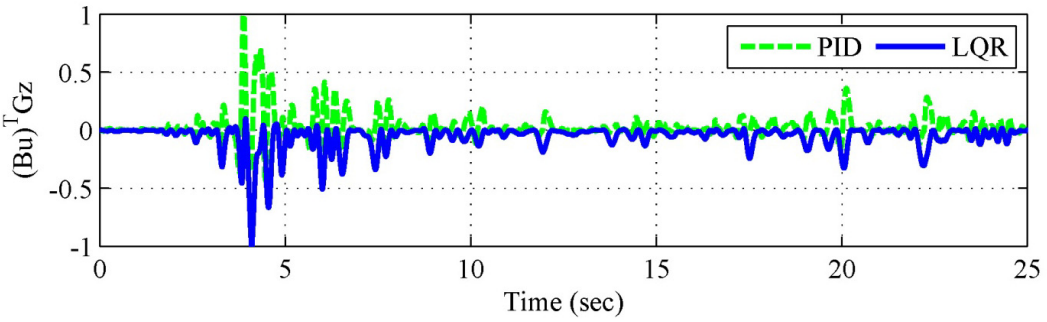

Figure 3-10. Time-history of the dissipativity constraint: Hachinohe earthquake.

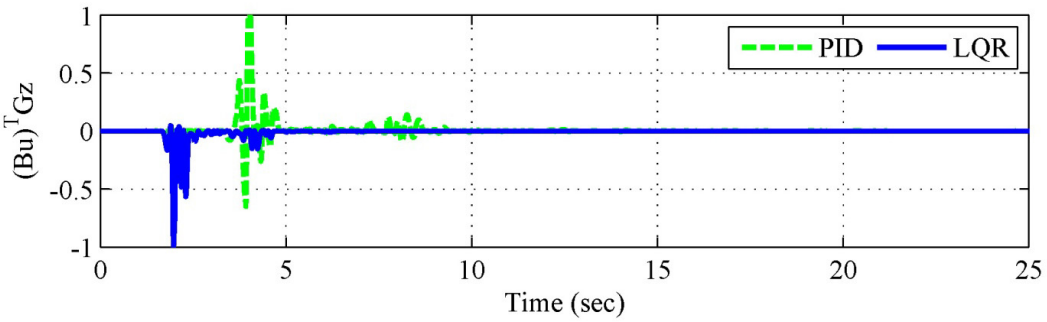

Figure 3-11. Time-history of the dissipativity constraint: Northridge earthquake.

3.7. Conclusion

In this chapter, a generalized deterministic definition for dissipativity of control forces is proposed. The proposed definition enables incorporating a dissipativity constraint to the design of dissipative optimal controllers. This definition is implemented in the design of an LQR optimal controller. A set of first-order optimality conditions are used to find the dissipative LQR optimal controller. Due to the specific nature of the proposed definition, the controller is found to be the commonly used LQR controller. Therefore,

LQR is found to be dissipative with respect to the generalized deterministic definition proposed, which verifies the advantage of clipped optimal control strategy with LQR as primary controller. This controller is consistent with the disipative nature of the semi-active damping devices and yields favorable performance. Simulation results demonstrate that the LQR effectively generates dissipative control forces for hazard mitigation of structures.

4. Summary

In this thesis, a new algorithm for system identification of smart structures called PANFIS is proposed which combines principal component analysis and adaptive neuro-fuzzy inference system. The main advantage of this algorithm is low computation time for modeling without much loss in accuracy due to data compression. In this thesis, a generalized deterministic definition for dissipativity of control variables is defined and used to prove the strict dissipativity of a LQR controller, supported by numerical simulation.

5. Recommendations and future work

In this thesis an efficient algorithm for system identification of smart structures is proposed. This method can be recommended to be implemented in control devices embedded in a large-scale smart structure for health monitoring to evaluate efficiency of the algorithm. The study on dissipativity of LQR controller can be expanded to a study of dissipativity of a smart damper, such as MR damper to evaluate its dissipative characteristic. Currently these exists no extensive experimental study of various smart dampers, which does not help spread the significant properties of these devices.

A combination of an efficient system identification algorithm and an analtically proven control method can also be suggested for further research. For example, application of PANFIS and LQR together seems to be promising, however, due to their differing formulations, combining them seems to be challenging.

6. References

Adeli H and Kim H 2004 “Wavelet-Hybrid Feedback-Least Mean Square Algorithm for Robust Control of Structures,” *Journal of Structural Engineering*, **130**(1): 128-137.

Avci E, Turkoglu I 2009 “An intelligent Diagnosis System Based on Principal Component Analysis and ANFIS for the Hearth Valve Diseases,” *Expert Systems with Applications*, **36**(2): 2873-2878

Avriel M. 1976 *Nonlinear Programming: analysis and Methods*. Prentice Hall Inc.

Bani-Hani K, Ghaboussi J and Schneider S P 1999 “Experimental Study of Identification and Control of Structures using Neural Network Part 1: Identification,” *Earthquake Engineering and Structural Dynamics*, **28**(9): 995-1018.

Chen Y, Yang B, Abraham A and Peng L 2007 “Automatic Design of Hierarchical Takagi-Sugeno Type Fuzzy Systems using Evolutionary Algorithms,” *IEEE Transactions on Fuzzy Systems*, **15**(3): 385-397.

Du H and Zhang N 2008 “Application of Evolving Takagi-Sugeno Fuzzy Model to Nonlinear System Identification,” *Applied Soft Computing*, **8**(1): 676-686.

Dyke S J, Spencer B F Jr, Sain M K and Carlson J D 1996 “Modeling and Control of Magnetorheological Dampers for Seismic Response Reduction,” *Smart Materials and Structures,* **5**(5): 565-575.

Dyke S J, Spencer B F Jr, Sain M K, Carlson J D 1998 “An Experimental Study of MR Dampers for Seismic Protection,” *Smart Materials and Structures*, 7(5):693–703.

Erkus B, Abe M, Fujino Y 2002 “Investigation of semi-active control for seismic protection of elevated highway bridges”. *Engineering Structures,* **24**(3):281–293.

Filev D P 1991 “Fuzzy Modeling of Complex Systems,” *International Journal of Approximate Reasoning*, **5**(3): 281-290.

Geering H P. 2007 *Optimal Control With Engineering Applications*. Springer.

Gopalakrishnan K and Khaitan S K 2010 “Finite Element Based Adaptive Neuro-Fuzzy Inference Technique for Parameter Identification of Multi-Layered Transportation Structures,” *Transport,* **25**(1): 58-65.

Gu Z and Oyadiji S 2008 “Application of MR Damper in Structural Control Using ANFIS Method,” *Computers & Structures,* **86**(3-5): 427-436

Housner G, Bergman L, Caughey T, Chassiakos A, Claus R, Masri S, Skelton R, Soong T, Spencer B, Yao J 1997 “Structural control: past, present, and the future,” ASCE *Journal*

of Engineering Mechanics, **123**(9): 897-971.

Hung S L, Huang C S, Wen C M and Hsu Y C 2003 "Nonparametric Identification of a Building Structure from Experimental Data using Wavelet Neural Network," *Computer-Aided Civil and Infrastructure Engineering*, **18**(5): 356-368.

Hurlebaus S and Gaul L 2006 "Smart Structure Dynamics," *Mechanical Systems and Signal Processing*, **20**(2): 255-281.

Inaudi J A 2000 "Performance of variable-damping systems: theoretical analysis and simulation," *Proceedings of 3rd International Workshop on Structural Control*, Paris, France, July 6-8, 2000; 301–316.

Jalili-Kharaajoo M 2004 "Nonlinear system identification using ANFIS based on emotional learning," *Lecture notes in computer science*, **3315**: 697-707

Jang J-S R 1993 "ANFIS: Adaptive-network-based Fuzzy Inference System," *IEEE Transactions on Systems, Man and Cybernetics* **23**(3): 665-685

Jang J-S R, Sun C-T, Mizutani E 1997 *Neuro-Fuzzy and Soft Computing,* Upper Saddle River, New Jersey, USA: Prentice Hall.

Johansen TA and Babuška R 2003 "Multiobjective Identification of Takagi-Sugeno Fuzzy Models," *IEEE Transactions on Fuzzy Systems*, **11**(6): 847-860.

Johansen T A 1994 "Fuzzy Model Based Control: Stability, Robustness, and Performance Issues," *IEEE Transactions on Fuzzy Systems*, 2(3): 221-234.

Johnson E A. 2000 "Nonlinear seismic benchmark problem: dissipativity and the 9-Story benchmark building," *Second European Conference on Structural Control (2ECSC)*, Champs-sur-Marne, France, July 3-6, 2000.

Johnson E A, Erkus B 2007 "Dissipativity and performance analysis of smart dampers via LMI synthesis," *Journal of Structural Control and Health Monitoring*, **14**:471-496.

Johnson E A, Baker G A, Spencer B F Jr, Fujino Y 2007 "Semiactive damping of stay cables," ASCE *Journal of Engineering Mechanics*, **133**(1): 1-11.

Jollife I T 2002 *Principal component analysis*, Springer.

Kim Y, Hurlebaus S and Langari R 2011 "MIMO Fuzzy Identification of Building-MR Damper System," *Journal of Intelligent and Fuzzy Systems,* **22**(4): 185-205

Kim Y, Hurlebaus S, Sharifi R and Langari R 2009 "Nonlinear Identification of MIMO Smart Structures," *ASME Dynamic Systems and Control Conference*, Oct. 12-14, Hollywood, California.

Kim Y and Langari R 2007 "Nonlinear Identification and Control of a Building Structure with a

Magnetorheological Damper System," *American Control Conference*, July 11-13, New York.

Kim Y, Langari R and Hurlebaus S 2009 "Semiactive Nonlinear Control of a Building with a Magnetorheological Damper System," *Mechanical Systems and Signal Processing*, **23**(2): 300-315.

Kuzniar K and Waszczyszyn Z 2006 "Neural networks and Principal Component Analysis for Identification of Building Natural Periods," j. Comput. Civ. Eng., **20**(6), 431-436

Langari R 1999 "Past, Present and Future of Fuzzy Control: A Case for Application of Fuzzy Logic in Hierarchical Control," in: *Proceedings*, *18th International Conference of the North American Fuzzy Information Processing Society-NAFIPS*, New York City, New York, USA, 760-765.

Lin J W and Betti R 2004 "On-line Identification and Damage Detection in Non-linear Structural Systems using a Variable Forgetting Factor Approach," *Earthquake Engineering and Structural Dynamics*, **33**(4): 419-444.

Mitchell R, Kim Y and El-Korchi T 2012 "System Identification of smart structures using a wavelet neuro-fuzzy model," *Journal of Smart Materials and Structures*, **21**(11): 1-12.

Mujica LE, Rodellar J, Fernandez A and Guemes A 2010 "Q-statistic and T2-statistic PCA-based measures for damage assessment in structures," *Structural Health Monitoring,* **10**(5): 539-553

Ozbulut O E, Mir C, Moroni M O, Sarrazin M, Roschke P N 2007 "A Fuzzy Model of Superelastic Shape Memory Alloys for Vibration Control in Civil Engineering Applications," *Smart Materials and Structures,* **16**(3): 818-829.

Palau C V, Arregui F J and Carlos M 2012 "Burst Detection in Water Networks Using Principal Component Analysis," *Journal of Water Resource Planning and Management,* **138**(1): 47-54

Park S, Lee J, Yun C, Inman D 2007 "Electro-Mechanical Impedance-Based Wireless Structural Health Monitoring Using PCA-Data Compression and *k*-means Clustering Algorithms," *Journal of Intelligent Material, Systems and Structures,* **19**(4): 509-520

Pearson K 1901 "On lines and planes of closest fit to systems of points in space," *Philosophical Magazine,* **2**(6): 559-572

Polat K, Gunes S 2007 "Automatic Determination of Diseases Related to Lymph System from Lymphography Data Using Principal Component Analysis (PCA), Fuzzy Weighting Pre-Processing and ANFIS" *Expert Systems with Application,* **33**(3): 636-641

Ramallo J C, Johnson E A, Spencer BF Jr 2002 " 'Smart' base isolation systems," ASCE *Journal of Engineering Mechanics*, **128**(10):1088–1099.

Ramallo J C, Yoshioka H and Spencer B F Jr. 2004 “A Two-step Identification Technique for Semiactive Control Systems,” *Structural Control and Health Monitoring*, **11**(4): 273-289.

Schurter K C and Roschke P 2000 “Fuzzy Modeling of Magnetorheological Damper Using ANFIS,” *The 9th IEEE International Conference on Fuzzy Systems,* May 2000, (1):122-127.

Sharifi R, Kim Y and Langari R 2010 “Sensor Fault Isolation and Detection of Smart Structures,” *Smart Materials and Structures*, **19**(10): 5001-5016

Smyth A W, Masri S F, Chassiakos A G and Caughey T K 1999 “On-line Parametric Identification of MDOF Nonlinear Hysteretic Systems,” ASCE *Journal of Engineering Mechanics*, **125**(2): 133-142.

Soong T T, Spencer B F Jr 2002 “Supplemental energy dissipation: state-of-the-art and state-of-the-practice,” *Engineering Structures*, **24**(3):243–259.

Spencer B F Jr., Dyke S J, Sain M K and Carlson J D 1997 “Phenomenological Model for Magnetorheological Dampers,” ASCE *Journal of Engineering Mechanics*, **123**(3): 230-238.

Spencer B F Jr, Johnson E A, Ramallo J C 2000 “ ‘Smart’ Isolation for Seismic Control,” JSME *International Journal Series C*, **43**(3):704–711.

Spencer B F Jr, Sain M K 1997 “Controlling Buildings: A New Frontier in Feedback,” IEEE *Control Systems Magazine*, **17**(6):19–35.

Symans M D, Constantinou M C 1999 “Semi-active Control Systems for Seismic Protection of Structures: a state-of-the-art Review,” *Engineering Structures,* **21**(6):469–487.

Takagi T and Sugeno M 1985 “Fuzzy Identification of Systems and Its Applications to Modeling and Control,” *IEEE Transactions on Systems, Man, and Cybernetics*, **15**(1): 116-132.

Wang L, Fu K 2009 *Artificial Neural Networks*, Wiley Encyclopedia of Computer Science and Engineering.

Wang H, Haiyan H 2009 “Hierarchical Fuzzy Identification of MR Damper,” *Proc. SPIE 7493*, *Second International Conference on Smart Materials and Nanotechnology in Engineering,* Oct. 2009, Weihai, China.

Wang L and Langari R 1995 “Decomposition Approach for Fuzzy Systems Identification,” in: *Proceedings*, *the 34th IEEE Conference on Decision and Control*, New Orleans, LA, USA, 261-265.

Warne K, Prasad G, Siddique N H, Maguire L P 2004 “Development of a Hybrid PCA-ANFIS Measurement System for Monitoring Product Quality in the Coating Industry” *Systems, Man and Cybernetics, IEEE international Conference,* Deny, UK, *Oct. 10-13,* **4**: 3519-3524.

Yager R R and Filev D P 1993 “Unified Structure and Parameter Identification of Fuzzy Models,” *IEEE Transactions on Systems, Man, and Cybernetics*, **23**(4): 1198-1205.

Yan G and Zhou L L 2006 “Integrated Fuzzy Logic and Genetic Algorithms for Multi-objective Control of Structures using MR Dampers,” *Journal of Sound and Vibration*, **296**(1-2): 368-382.

Yang G, Spencer B F Jr., Carlson J D and Sain M K 2002 “Large-scale MR Fluid Dampers: Modeling and Dynamic Performance Considerations,” *Engineering Structures*, **24**(3): 309-323.

Yang JN. 1982 “Control of tall building under earthquake excitation,” *Journal of Engineering Mechanics Division*, **108**(EM5), 833-49

Yang Y N and Lin S 2004 “On-line Identification of Non-linear Hysteretic Structures using an Adaptive Tracking Technique,” *International Journal of Non-Linear Mechanics*, **39**(9): 1481-1491.

Yang Y N and Lin S 2005 “Identification of Parametric Variations of Structures based on Least Squares Estimation and Adaptive Tracking Technique,” ASCE *Journal of Engineering Mechanics*, **131**(3): 290-298.

Yen J and Langari R 1998 *Fuzzy Logic-Intelligence, Control, and Information*, Upper Saddle River, New Jersey, USA: Prentice Hall.

Zadeh L A 1965 “Fuzzy Sets,” *Information and Control*, **8**(3): 338-353.